Uncertainties associated to measurements of inherent optical properties in natural waters

Edouard Leymarie,* David Doxaran, and Marcel Babin

Université Pierre et Marie Curie, Laboratoire d'Océanographie de Villefranche, Centre National de la Recherche Scientifique, Villefranche-sur-Mer, France

*Corresponding author: leymarie@obs-vlfr.fr

Received 5 April 2010; revised 23 July 2010; accepted 10 August 2010; posted 30 August 2010 (Doc. ID 126477); published 28 September 2010

Monte Carlo simulations are used to explain and quantify the errors in inherent optical properties (IOPs) (absorption and attenuation coefficients) measured using the WET Labs AC-9 submarine spectrophotometer, and to assess correction algorithms. Simulated samples with a wide range of IOPs encountered in natural waters are examined. The relative errors on the measured absorption coefficient are in general lower than 25%, but reach up to 100% in highly scattering waters. Relative errors on attenuation and scattering coefficients are more stable, with an underestimation mainly driven by the volume scattering function. The errors in attenuation and scattering spectral shapes are small. © 2010 Optical Society of America

OCIS codes: 010.4450, 120.6200.

1. Introduction

The inherent optical properties (IOPs), such as the absorption, attenuation, and scattering coefficients, determine the propagation of light within natural waters. In the visible part of the spectrum, the availability of solar light controls the rate of primary production (photosynthesis), photodegradation of the organic matter, and, to some extent, the bacterial activity, and thus directly impacts the ecosystem. Accurate knowledge of the IOPs is also essential for ocean color remote sensing applications, for algorithm development, and for calibration and validation of satellite products [1], over the ultraviolet, visible, and near-infrared (near-IR) parts of the light spectrum.

In situ measurements of the IOPs are required to address these questions. Field spectrophotometers, such as the AC-9 (WET Labs, Inc.), have been developed during the last two decades and are widely used in oceanic, coastal, estuarine, and lake waters. The attenuation (c, in m^{-1}) and absorption (a, in m^{-1}) coefficients (see Table 1 toward the end of the paper for a detailed list of symbols) of the water sampled are measured simultaneously by using a spectrophotometer equipped with two different "optical tubes" that contain the water sample, while the scattering coefficient (b in m^{-1}) is not directly measured but is estimated from these two parameters. However, the accurate measurement of the absorption coefficient in the field is almost impossible because of the difficulty of desiging sensors that fully collect all the scattered photons. The solution adopted for the AC-9 is to correct absorption measurements from residual scattering effects. The widely used correction method, proposed by Zaneveld *et al.* [2], relies on several assumptions that have never been fully tested. The direct consequence is that existing IOP datasets are associated with unknown uncertainties that may be high enough to lead to erroneous analyses and conclusions in the fields of marine optics and ocean color remote sensing.

In this study, we use a new Monte Carlo code to understand and quantify the errors associated with field measurements of the IOPs of natural waters. The design of the AC-9 spectrophotometer is simulated and the method currently proposed to correct for residual scattering effects is applied. The issues related to the optical design of the instrument and to

0003-6935/10/285415-22$15.00/0

the scattering correction method of Zaneveld *et al.* [2] are investigated for a wide range of IOPs in order to provide results usable in most of the natural waters (from clear to highly turbid waters). We quantify the errors on the c, a, and b coefficients and on associated spectral shapes, in the visible and near-IR spectral regions (400–900 nm). Most of the results are presented for an AC-9 device with a and c-tube lengths of 10 cm, but the influence of the tube length (either 10 or 25 cm for such a device) is also examined.

2. Background

A. Measurement Principles

The WET Labs AC-9 [3] and AC-S spectrophotometers [9 indicates the number of wavelengths and S stands for (hyper)spectral] are equipped with optical flow tubes filled with natural water, which is either pumped or passed manually by gravity. At one extremity of the tube, a collimated light source is filtered through bandpass filters to create a narrowband spectral output. A receiver detector, characterized by its field of view (FOV) in water, is positioned at the other extremity of the tube. Measurements of the c and a coefficients are achieved based on the Beer–Lambert law, which describes the variation of light emitted from a source with an intensity I_0 (in W m^{-2}) along a path length L (in meters):

$$x = -\frac{1}{L}\ln\left(\frac{S_x}{I_0}\right), \tag{1}$$

where S_x is the detected light intensity and x is the variation coefficient, in m^{-1}.

Light traveling along the path is subject to both scattering and absorptive losses. In the case of a "black" tube, the scattered light that hits the blackened surface of the flow tube is absorbed. If the detector FOV is narrow enough, x is approximately equal to the attenuation (absorption + scattering) coefficient of the medium (c, in m^{-1}). If the surface of the flow tube is fully reflective and the detector FOV is wide, the scattered light will remain in the tube so that the variation of light intensity that will be measured mostly results from absorptive losses. In this case, x is approximately equal to the absorption coefficient of the medium (a, in m^{-1}). The simultaneous measurement of a and c allows determining the scattering coefficient of the medium, b in m^{-1}, as

$$b = c - a. \tag{2}$$

The absorption and attenuation signals measured are both referenced to pure water. The spectrophotometer is calibrated in the laboratory prior to deployment in the field, based on Eq. (1), so that the variation of light actually measured, x_m in m^{-1}, can be written as

$$x_m = -\frac{1}{L}\ln\left(\frac{S_x}{I_0}\right) + \frac{1}{L}\ln\left(\frac{S_{x,w}}{I_0}\right) = x - x_w, \tag{3}$$

where x, x_w, and x_m, in m^{-1}, are, respectively, the total, pure water, and measured variation coefficients (here a or c). Therefore, the measured light variation results from the contributions of the colored water constituents on top of pure water.

B. Measurement Errors and Corrections

Two distinct sources of measurement errors must be considered separately. The first source mainly results from pure water calibration of the instrument, while the second source is inherent to the instrument itself.

Error in AC-9 and AC-S determinations of a and c is associated with uncertainties in pure water calibration [Eq. (3)]. A pure water calibration of the spectrophotometer is made at specific temperature and salinity (typically 20 °C and 0 PSU). As light absorption and attenuation by pure water are sensitive to temperature and salinity, these two parameters must be measured in the field coincidently with optical data. Temperature and salinity corrections are then applied to raw data measured in the field using spectral temperature and salinity correction factors provided by the constructor and/or the literature [4–6]. Frequent laboratory calibrations (with regard to pure water) of the sensor and accurate field measurements of water temperature and salinity are required to minimize these errors. Moreover, improper use of the AC-9 could lead to the presence of air bubbles or turbulence, which may affect the measurement accuracy. Although this study does not focus on these errors, which are specific to the conditions of use, they should be carefully taken into account by users during field experiments.

The errors inherent of the instrument itself, which are investigated in our study, result from the method and the geometry used to measure the optical properties. Errors that depend on the electronics of the AC-9 instrument, like saturation or sensibility limitations, are not taken into account in this work. Error sources studied here differ for absorption and attenuation measurements. The main source of error when measuring the absorption coefficient is related to light scattering and is twofold [7]. The first error results from the increase of the actual photon path length [L in Eq. (1)] in the flow tube because of single and multiple scattering and leads to an overestimation of a. The second error occurs because part of the scattered light is not detected (or lost) and is confounded with absorbed photons. This error is induced by most photons reaching the wall with an angle higher than 41.7° (the critical angle for total internal reflection at the quartz–air interface) in the case of the WET Labs AC-9 sensor. Beyond this angle, the internal reflection coefficient decreases rapidly to a few percents within a few degrees; therefore, photons are assumed to be lost, i.e., not detected. This results in the overestimation of a.

When measuring the attenuation coefficient, the increase of the photon path length due to the occurrence of single and multiple scattering may

represent a source of error. However, previous studies [8,9,7] have shown that the measurement error mainly results from photons scattered in the forward direction with an angle lower than the FOV of the detector. Based on information provided by WET Labs, the receiver FOV in the c-tube of the AC-9 sensor is 0.9°. This leads to an underestimation of c. For this reason, the error on c is logically minimized when the FOV tends toward 0 [10]. This problem is particularly important when dealing with seawater samples, as the volume scattering function (VSF) is always highly peaked in the forward direction.

Both absorption and attenuation measurements carried out with the AC-9 and AC-S sensors are thus associated with errors due to scattering. This leads to systematic overestimation of a and underestimation of c. This statement can be expressed by the following equations proposed by Zaneveld *et al.* [2]:

$$a_m(\lambda) = a_t(\lambda) + k_a(\lambda) \times b_t(\lambda), \tag{4}$$

$$c_m(\lambda) = c_t(\lambda) - k_c(\lambda) \times b_t(\lambda), \tag{5}$$

where the subscripts m and t stand for measured and true. As first approximations, k_a is the fraction of light scattered in the a-tube with an angle higher than 41.7°, i.e., not detected in the absorption flow tube (and therefore erroneously accounted for as absorbed); k_c is the fraction of the scattered light captured within the FOV of the detector in the c-tube, i.e., detected in the attenuation flow tube (and therefore erroneously not accounted for as scattered).

While the measurement error in the c-tube is explicit in Eq. (5), Zaneveld *et al.* [2] do not provide any scattering correction method for the c coefficient. These authors suggest three possible corrections to take into account the scattering error on the a-tube. The method called "proportional correction" is expected to be the most accurate. Our results confirm this statement (not shown), so that only results obtained when applying the "proportional correction" are presented here. This method relies upon several assumptions summarized hereafter.

The first assumption is that the fraction of scattered photons not collected by the absorption tube [k_a in Eq. (4)] is independent of wavelength. The same assumption is made for the fraction of scattered photons collected by the attenuation flow tube, i.e., k_c is also assumed to be independent of wavelength in Eq. (5). Based on these two hypotheses, Zaneveld *et al.* [2] show that, for any set of two wavelengths λ_1 and λ_2,

$$\frac{b_m(\lambda_1)}{b_m(\lambda_2)} = \frac{b_t(\lambda_1)}{b_t(\lambda_2)}. \tag{6}$$

The third assumption states that there is a reference wavelength in the near-IR part of the spectrum, noted λ_r, where light absorption by the colored water constituents (other than pure water or seawater) is negligible. The combination of these three assumptions provide a scattering correction for the measured absorption values, thus a corrected absorption coefficient, noted a_c, is

$$a_c(\lambda) = a_m(\lambda) - a_m(\lambda_r) \times \frac{b_m(\lambda)}{b_m(\lambda_r)}. \tag{7}$$

The advantage of this correction method is that it only requires AC-9 measurements. Based on Eqs. (4), (5), and (7), the uncertainties associated with c_m and a_c may vary with the IOPs. Moreover, these uncertainties depend on the validity of the underlying assumptions [k_a and k_c are wavelength independent and $a_t(\lambda_r)$ is equal to zero]. In the current study, a Monte Carlo code is used to assess the validity of these assumptions and estimate the uncertainties associated with c_m and a_c in various natural waters.

3. Methods

A. Monte Carlo Code

SimulO (www.obs-vlfr.fr/LOV/OMT/SimulO/) is a new Monte Carlo code developed to easily simulate many types of optical devices, especially in the field of marine optics. It is a natural three-dimensional (3D) forward Monte Carlo code, which implies that each photon is followed, one at a time, from the source to the point where it is absorbed.

Using SimulO, complex optical devices can be virtually created by positioning and sizing any number of elementary virtual objects. Photon intersections with objects are carried out analytically, and specific topological rules are used to create a given setup by adding objects. Currently, three elementary shapes are available: spheres, cubes, and cylinders. The volume occupied by each elementary object is homogenous in terms of bulk optical properties, while different optical properties can be ascribed to each face of the object. The optical setup includes four parameters: (i) the refractive index of the material (used for the calculation of Snell's and Fresnel's laws), (ii) the absorption and (iii) scattering coefficients, and (iv) the scattering phase function. For the latter, the user can either select one of the built-in phase functions (pure water, isotropic, Henyey–Greenstein, Fournier–Forand) or upload from a file a more specific function, which will be interpolated to the appropriate angles. To simulate a volume with two different types of scatterers (e.g., water and particles), SimulO accommodates the use of two scattering functions that can be weighted with their respective scattering probability by setting different scattering coefficients. The optical properties used to describe each face of an elementary object (bidirectional reflectance function) can be set to transparent, specular, or Lambertian reflection (with a given reflection probability). The face of any object can also be defined as a light source. In this case, photons are emitted from points randomly distributed over the area, with a direction relative to the local normal to the face. The user can specify whether the angular direction of an emitted photon is (i) normal to the

face, (ii) Lambertian, or (iii) randomly distributed with a given divergence around the normal direction. By default, SimulO records the number of collisions on each face of the elementary objects, the average path length of photons, the average number of scattering events per photon, and the number of photons absorbed within the volume and on each face of an object. Optional specific tools also allow knowing the average path length of photons absorbed by a specific face, the angular distribution of photons reaching a specific face, and the number of photons reaching a specific face within a specified angular range.

The SimulO code was validated based on other published Monte Carlo simulations in marine optics. Some of these intercomparison exercises are summarized hereafter. The first geometry tested was that of a point source integrating cavity absorption meter (PSICAM) [11,12]. The PSICAM was modeled as a sphere with the appropriate radius and its internal face was set to a Lambertian reflector (with the given reflectivity of the modeled material). The bulk properties were set to those of the water sample studied. Another small sphere with an external face set as a photon emitter was placed at the center of the first sphere. SimulO reproduced the theoretical equation for both the average path length and number of collisions on the internal face of the cavity when the sample is purely absorbent (see Eqs. 4 and 5 in [11]) with differences smaller than 0.4%. Leathers *et al.* [12] also used Monte Carlo simulations to determine the error in the PSICAM response due to the presence of scatterers with isotropic and Petzold phase functions [13], for different values of the absorption coefficient (see their Figs. 2 and 3). For both cases, SimulO reproduced Leathers *et al.*'s results with differences equal to the statistical error of Monte Carlo simulations when considering 10^7 emitted photons. The second geometry tested was a reflective tube absorption meter as simulated by Kirk [14]. To understand the behavior of a reflective absorption tube, this author studied the variations of the ratio between the measured and true absorption coefficients as a function of the acceptance angle of the detector and of the tube reflectivity (see Figs. 2 and 3 in this paper). Kirk's [14] results were reproduced with SimulO with a difference smaller than 0.5%. Additional cases with other absorption and scattering coefficients (with comparable geometry) were also simulated and compared to results obtained with published Monte Carlo codes [7] with differences smaller than a few percent. SimulO was also used to simulate the propagation of light within a water column. The code perfectly reproduced results obtained by Mobley *et al.* [15] (see their canonical problems numbered 2 and 3).

B. Modeling the Absorption and Attenuation Meters

The geometrical and optical properties of the *a*- and *c*-tubes of the AC9 device were set based on information kindly provided by the WET Labs technical staff (Fig. 1). A 3D modeling was used (as our SimulO code only works with a 3D scheme), but a two-dimensional representation would have been suitable due to the axial symmetry of the AC-9 device.

The modeled *a*-tube is composed of a source, a tube, and a detector. The source is modeled as a cylinder with a radius of 0.315 cm located at 9.036 cm back from the water side of the quartz input window. The tube length is set to 10 cm, as such a short path length is more appropriate for measuring the optical properties of both clear and turbid waters. Photons are emitted with a divergence angle of 0.95° (half angle). Two quartz windows (0.5 cm thick each) exactly 10 cm distant from each other are positioned at both ends of a quartz tube (8.5 cm length) with an inner radius of 0.6 cm and an outer radius of 0.75 cm. This tube is used to collect the scattered light and reflect it back within the water sample and toward the detector. To bridge this quartz tube and the two quartz windows, two tubes with fully absorbent walls are added. In the real absorption tube, the air side of the exit quartz window is covered by a thin layer of optical epoxy with a scattering material added to it. This scattering layer is immediately followed by a large silicon diode. This technique, used to increase the acceptance angle of the detector, cannot easily be modeled with SimulO. Therefore, we used a cylinder shape with a radius of 1.4 cm, separated

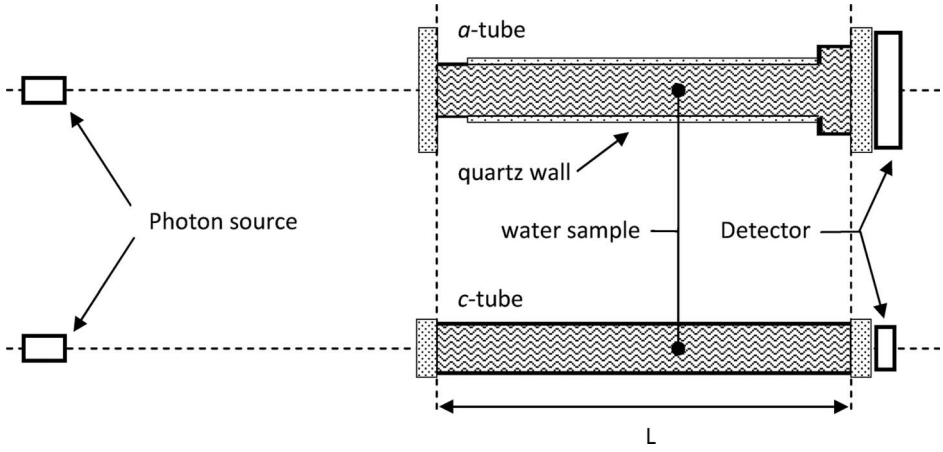

Fig. 1. Schematic modeling of the absorption and attenuation tubes including the light sources and detectors.

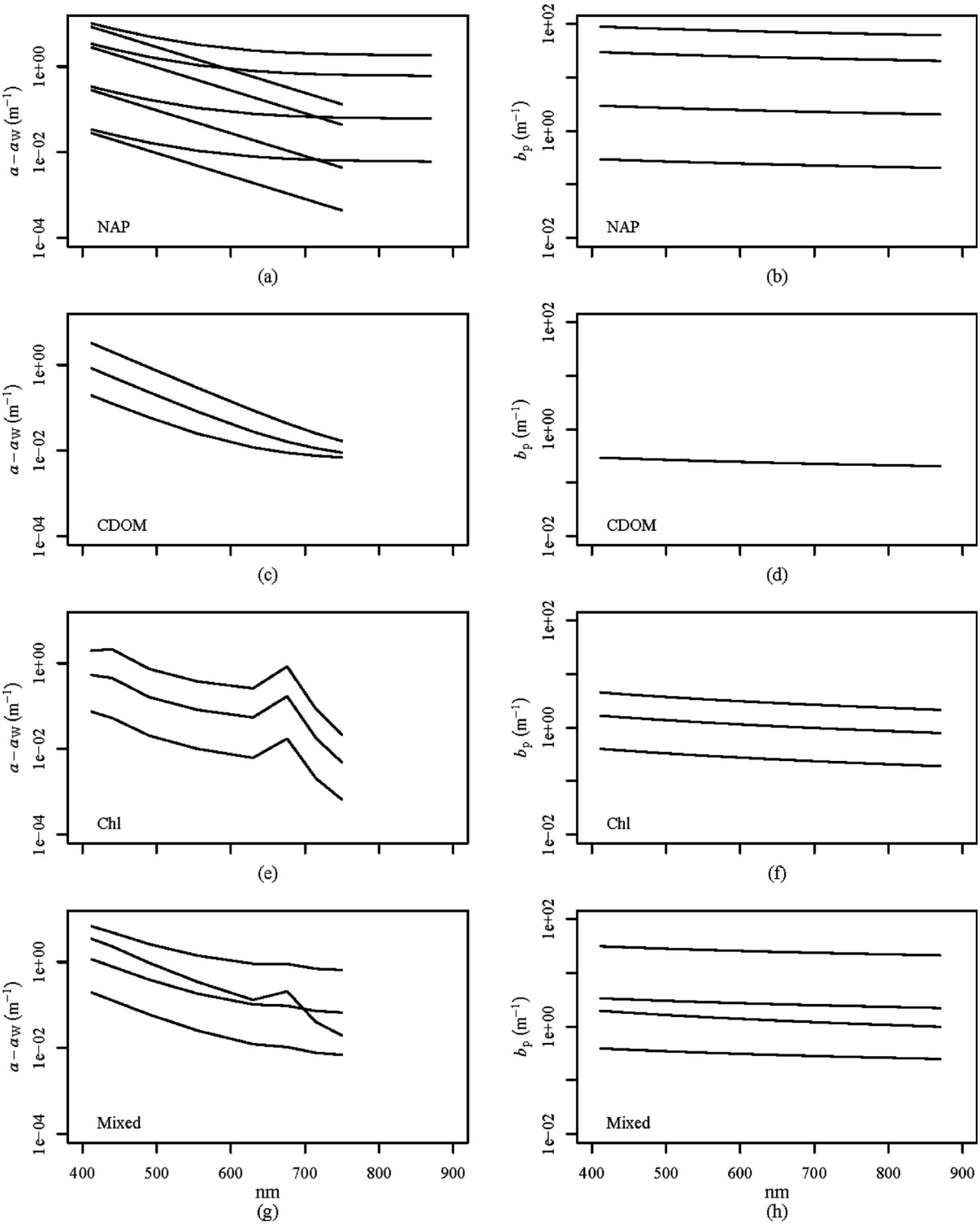

Fig. 2. Modeled IOP dataset used as inputs for Monte Carlo simulations. Absorption coefficients are cut at 767 nm because of null value at 870 nm (in log scale).

from the exit window by a thin layer of air, to represent the detector collecting area. This detector has an acceptance angle of 60° (half angle), which means that only the photons reaching the detector with a polar angle smaller than 60° will be detected, i.e., counted. This value of 60° is somewhat arbitrary, but previous studies [14,16] showed that the exact value of the detector acceptance angle is not significant beyond 45° (half angle). All faces of this virtual detector are set to be fully absorbent. Therefore, only photons that are reflected by the quartz–air interface can go back within the tube.

The *c*-tube is easier to model. The photon source is the same as in the *a*-tube and is also located at a

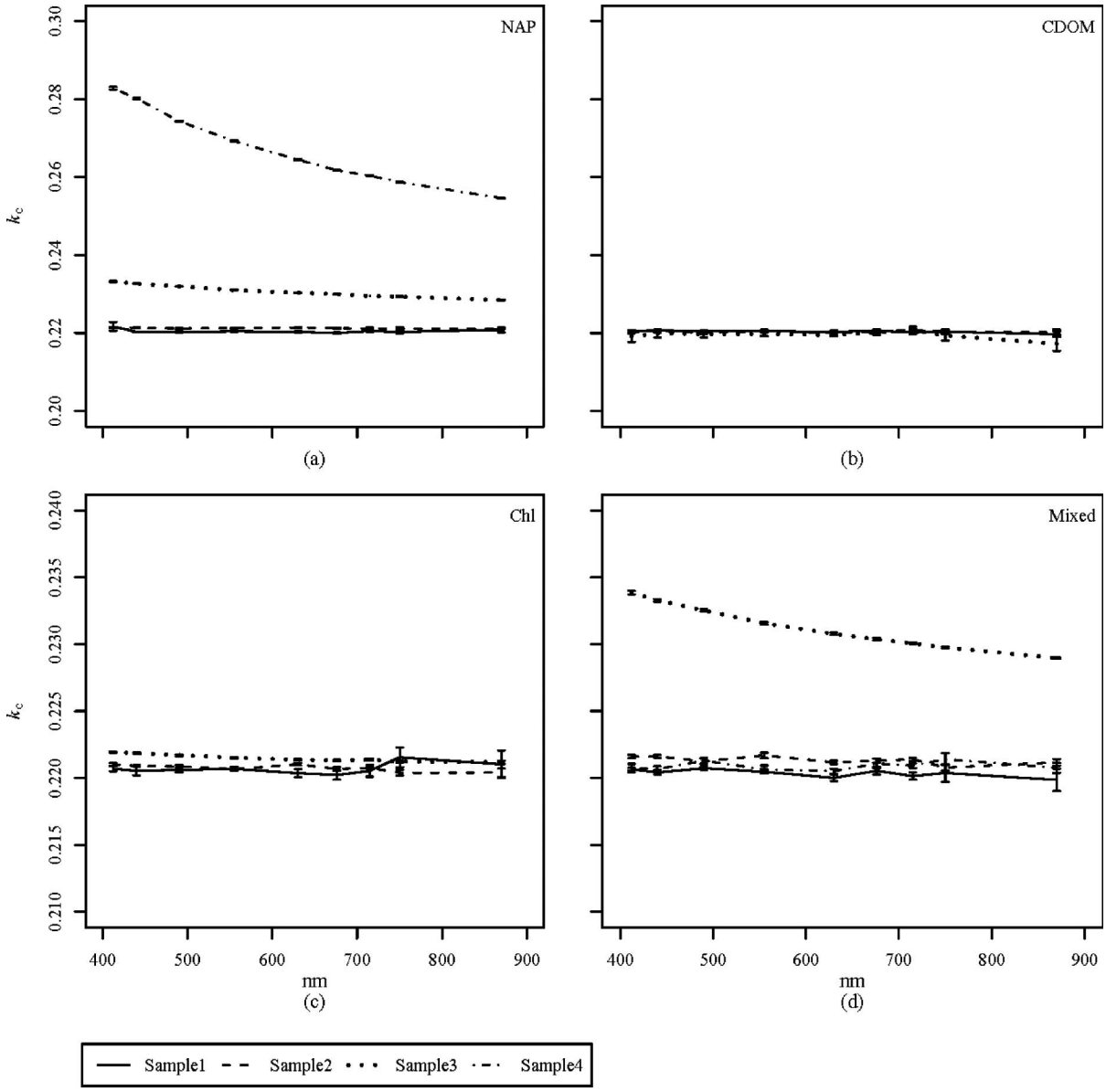

Fig. 3. Spectral variations of k_c in (a) NAP-dominated, (b) CDOM-dominated, (c) Chl-dominated, and (d) Mixed natural waters. For each water type, results are presented for sample1 to sample4. The AC-9 tube length is 10 cm, and the VSF used is FF-183.

distance of 9.036 cm away from the water side of a quartz window (0.5 cm thick). This window is followed by a tube with a radius of 0.6 cm and a length of 10 cm. The volume inside the tube has the bulk properties of the water sample studied while the wall of the tube is set to fully absorbent. A second 0.5 cm thick quartz window closes the tube and is immediately followed by a cylinder that represents the detector. This detector has a diameter of 1.04 cm and an acceptance angle of 1.2° (half angle). This acceptance angle in the air, derived from the optical design given by WET Labs, corresponds to an acceptance angle of 0.9° in water. As for the absorption tube, only photons that are reflected by the quartz–air interface at the exit window can go back within the tube.

During a simulation, the probability of detection, noted P, is calculated as the number of photons reaching the detector inside the FOV divided by the number of photons emitted. This calculation is performed for each tube separately and for each set of optical properties $a_t(\lambda)$ and $b_t(\lambda)$ ascribed to a water sample. As for real AC-9 measurements, these optical properties are referenced to pure water. For this reason, the probability of detection (P_0) is initially computed with the tubes filled with pure water. The pure water absorption coefficient is taken from Pope and Fry [17] between 380 and 725 nm and from Kou *et al.* [18] between 730 and 900 nm. The pure seawater scattering coefficient and phase function are taken from Morel [19]. A very recent study provides new values for the pure seawater scattering coefficient [20]. These values are actually very close to the ones of Morel [19] (within 1%) and, due to the high values of the ratio b_t/b_w considered in our study

(minimum 45 and up to 230,000), do not significantly affect our results.

Based on Eq. (3), the absorption and attenuation coefficients that would be measured with the simulated AC-9 sensor, noted $a_m(\lambda)$ and $c_m(\lambda)$, respectively, are calculated as

$$x_m(\lambda) = -\frac{1}{L}\ln\left(\frac{P^x_{a_t,b_t}(\lambda)}{P^x_{0,0}(\lambda)}\right), \tag{8}$$

where x is either a or c, and $P^x_{a_t,b_t}(\lambda)$ and $P^x_{0,0}(\lambda)$ are, respectively, the probabilities of detection computed for the water sample and for pure water.

The true (imposed) optical properties for a water sample are $a_t(\lambda)$ and $b_t(\lambda)$, then $c_t(\lambda)$ is equal to $a_t(\lambda) + b_t(\lambda)$. Computations with SimulO give the optical properties that would be measured by the AC-9, noted $a_m(\lambda)$ and $c_m(\lambda)$. The actual values of $k_a(\lambda)$ and $k_c(\lambda)$ are obtained from Eqs. (4) and (5), respectively. The method proposed by Zaneveld *et al.* [2] to correct for residual scattering is strictly applied to obtain the corrected absorption $a_c(\lambda)$ and scattering $[b_c(\lambda) = c_m(\lambda) - a_c(\lambda)]$ coefficients. The relative errors, in percent, associated with the measured $c_m(\lambda)$, $a_c(\lambda)$ and $b_c(\lambda)$ coefficients are calculated as

$$E_x(\lambda) = \left(\frac{x_m(\lambda) - x_t(\lambda)}{x_t(\lambda)}\right) \times 100, \tag{9}$$

where x_m is either a_c, c_m, or b_c.

C. Modeled Water Samples

The following wavelengths were considered in the computations: 412, 440, 490, 555, 630, 676, 715, 750, and 870 nm. These wavelengths, available for AC-9 sensors, were selected in order to cover the visible and near-IR spectral domains, and also to match the absorption peaks of phytoplankton centered at 440 and 675 nm. The spectral variations of k_a and k_c and the spectral errors associated with the simulated absorption and attenuation coefficients were calculated using SimulO, considering a wide range of optical properties representative of most natural waters. These optical properties were obtained by mixing the additive separate contributions, in terms of absorption and scattering, of the three following broad classes of optically significant constituents found in natural waters: phytoplankton (Chl), colored dissolved organic matter (CDOM), and nonalgal particles (NAP). The respective absorption and scattering coefficients, in m^{-1}, were calculated by using the following parameterizations for the individual components. For phytoplankton absorption [21],

$$a_{\mathrm{Chl}}(\lambda) = [\mathrm{Chl}] \times a^*_{\mathrm{Chl}}(\lambda), \tag{10}$$

where $a_{\mathrm{Chl}}(\lambda)$ is the absorption coefficient of phytoplankton (m^{-1}), [Chl] is the total concentration of chlorophyll-a and phaeopigments (mg m^{-3}), and $a^*_{\mathrm{Chl}}(\lambda)$ is the chlorophyll-specific absorption coefficient of phytoplankton (m^2(mg Chl)$^{-1}$). In the visible spectral domain, the $a^*_{\mathrm{Chl}}(\lambda)$ values used in the computations were taken from Bricaud *et al.* [22] for [Chl] concentrations ranging from 1 to 10 mg m^{-3} and from Dall'Olmo and Gitelson [23] for higher [Chl] concentrations. The $a^*_{\mathrm{Chl}}(870)$ value was systematically set to 0, while $a^*_{\mathrm{Chl}}(715)$ and $a^*_{\mathrm{Chl}}(750)$ were obtained from a linear interpolation between 700 and 870 nm.

Light scattering by phytoplankton was modeled as [24]

$$b_{\mathrm{Chl}}(\lambda) = 0.3 \times [\mathrm{Chl}]^{0.62} \times (550/\lambda). \tag{11}$$

Light absorption by CDOM was assumed to fit an exponential function [25]:

$$a_{\mathrm{CDOM}}(\lambda) = a_{\mathrm{CDOM}}(440) \times \exp(-0.017 \times (\lambda - 440)), \tag{12}$$

with a mean spectral slope of 0.017 nm^{-1} [26].

Light absorption by NAP was modeled using a similar exponential function [27]:

$$a_{\mathrm{NAP}}(\lambda) = [\mathrm{NAP}] \times a^*_{\mathrm{NAP}}(440) \times \exp(-0.0123 \times (\lambda - 440)), \tag{13}$$

where [NAP], in g m^{-3}, is the concentration of NAP, and $a^*_{\mathrm{NAP}}(440)$ is the mass-specific absorption coefficient of NAP (set to a constant value of 0.04 m^2 g^{-1} [28]). The value of the spectral slope used in our computations (0.0123 nm^{-1}) is the average value found for European coastal waters [26]. In all the cases simulated, $a_{\mathrm{Chl}}(870)$, $a_{\mathrm{CDOM}}(870)$, and $a_{\mathrm{NAP}}(870)$ were set equal to 0, and Eqs. (10), (12), and (13) were used to model light absorption by the optically active water constituents at the other wavelengths. This implies that one of the main assumptions made in the correction proposed by Zaneveld *et al.* [2] [Eq. (7)] was fulfilled at 870 nm, but not at the other near-IR wavelengths considered here (715 and 750 nm).

Finally, light scattering by NAP particles was modeled using the following power-law function [29]:

$$b_{\mathrm{NAP}}(\lambda) = [\mathrm{NAP}] \times b^*_{\mathrm{NAP}}(555) \times (\lambda/555)^{-0.5}, \tag{14}$$

where $b^*_{\mathrm{NAP}}(555)$ is the mass-specific scattering coefficient of NAP, set to a constant value of 0.51 m^2 g^{-1} [28]. The mean value of the scattering spectral slope (0.5) was selected based on results obtained by Doxaran *et al.* [30].

The optical properties of the modeled water samples, $a_t(\lambda)$ and $b_t(\lambda)$, were obtained as the sum of the phytoplankton, CDOM, and NAP contributions. The complete set of modeled spectral absorption and scattering coefficients considered is presented in Fig. 2. The objective was to reproduce typical inherent optical properties encountered in so-called Case 1 and Case 2 waters [31], i.e.:

i. in oceanic waters with various concentrations of chlorophyll pigments, including concentrations reached during phytoplankton blooms; the case of high concentrations of Chl and CDOM (resulting from phytoplankton decay) and low concentration of NAP (detrital suspended matter) was also considered as it was encountered in highly productive lake waters [23]; and

ii. in coastal and estuarine waters with various Chl concentrations and systematic high concentrations of terrigenous substances in solution (CDOM) and/or in suspension (NAP). The concentrations considered for these two last water constituents were documented during field experiments [23,26,28,32].

Fourteen modeled water samples were generated and classified into four distinct categories of natural waters (Table 2).

i. Typical Chl-dominated Case 1 waters, i.e., pure seawater with increasing [Chl] concentrations: 1, 10, and 50 mg m^{-3} (samples noted Chl1 to Chl3). The [NAP] concentrations were set to obtain a a_{NAP}: $a_{Chl}(440)$ ratio that varies according to [33], which corresponds to 47, 21, and 12%, respectively, for samples Chl1, Chl2, and Chl3. The [CDOM] concentrations were set to obtain a constant a_{CDOM}: $a_{Chl}(440)$ ratio of 30% [21]. The case of an extremely low [Chl] concentration was not considered due to the too long computation time necessary to reach convergence (see below). Here b_t was simply modeled using Eq. (11), as it includes light scattering by all particles found in Case 1 waters.

ii. Case 2 NAP-dominated waters, i.e., pure seawater with increasing [NAP] concentrations: 0.5, 5, 50, and 150 g m^{-3} (samples noted NAP1 to NAP4).

iii. Case 2 CDOM-dominated waters, i.e., pure seawater with increasing CDOM [$a_{CDOM}(440)$] concentrations: 0.1, 0.5, and 2 m^{-1} and a fixed NAP concentration of 0.5 g m^{-3} (samples noted CDOM1 to CDOM3).

iv. Case 2 waters with mixed contributions of Chl, CDOM, and NAP: (0.1 mg m^{-3}, 0.1 m^{-1}, 0.5 g m^{-3}), (1 mg m^{-3}, 0.5 m^{-1}, 5 g m^{-3}), (10 mg m^{-3}, 2 m^{-1}, 50 g m^{-3}), and (10 mg m^{-3}, 2 m^{-1}, 0.5 g m^{-3}). These four samples are noted Mixed1 to Mixed4.

For the VSF of particles, we considered a spectrally flat Fournier–Forand phase function [34] with a fixed backscattering ratio [35] independently of the simulated water type. A backscattering ratio of 1.83% was used to be consistent with other Monte Carlo studies using the VSF measured by Petzold [13].

D. Estimation of Computation Errors

The Monte Carlo approach is a statistical method that randomly simulates the propagation of millions of photons to estimate an average behavior. It is, therefore, always important, prior to any result interpretation, to assess the precision (i.e., convergence) of a simulation. In the current study, the problem of convergence is critical because different simulation results, such as the error on the absorption measurement retrieved by the proportional correction method [Eq. (7)], combine several simulations (for the a- and c-tubes, for the sample and for pure water, at the selected wavelength and the near-IR reference wavelength). The precision for a computation was calculated as follows. For each case considered (i.e., a selected tube, wavelength, and set of IOPs), hundreds of simulations (each one corresponding to 10^7 photons emitted) were run. Results from these simulations were randomly classified, then averaged into ten groups, i.e., ten replicates of the same case. If the number of photons used was high enough, the difference between replicates should be negligible. These replicates were then averaged to obtain the final result. The computation error was calculated as the standard deviation over these replicates divided by the square root of 10 (the number of replicates) to take into account that final results were obtained with 10 times more photons than each replica.

4. Results and Discussion

A. Error on the Measured Attenuation Coefficient

Based on Eq. (5), the measurement error on c_t depends on k_c and b_t. As a first approximation, k_c can be obtained by simply integrating the normalized VSF over the FOV of the detector. In the case of the selected VSF (FF-183), this integral is equal to 24%. Results from SimulO are presented separately for the four types of natural waters considered (NAP dominated, CDOM dominated, Chl, and Mixed) (Fig. 3). Between 412 and 870 nm, the simulated k_c is equal to about 22% and remains lower than the first approximation of 24% as long as b_t is lower than 30 m^{-1} (samples NAP3 and Mixed3), which is the case in most natural waters, apart from highly turbid resuspension zones, estuaries, and river plumes. The fact that simulated values are lower than theoretical ones results from the divergence of the light source. Indeed, when considering a perfectly parallel beam, theoretical and simulated k_c values do not differ except in highly turbid conditions (results not shown). A significant increase in k_c (values up to 28%) only occurs when b_t reaches extreme values close to 100 m^{-1} (sample NAP4) because of significant multiple scattering effects [7]. As expected [2], results show very limited spectral variations of k_c whatever the water type considered. Only sample NAP4 exhibits more pronounced k_c spectral variations (+11% from 870 to 412 nm). These first results show the limited influences of the water turbidity and wavelength on k_c. Note, however, that the actual variations of k_c are expected to be mainly affected by the angular variations of the particulate VSF [8,9,7,10]. Such cases are considered later in Subsection 4.D.

As long as k_c is almost a constant value of 22%, the measured c_m coefficient underestimates by 22% the actual c_t value (Fig. 4). This simple result is implicit from Eq. (5) when scattering predominates over

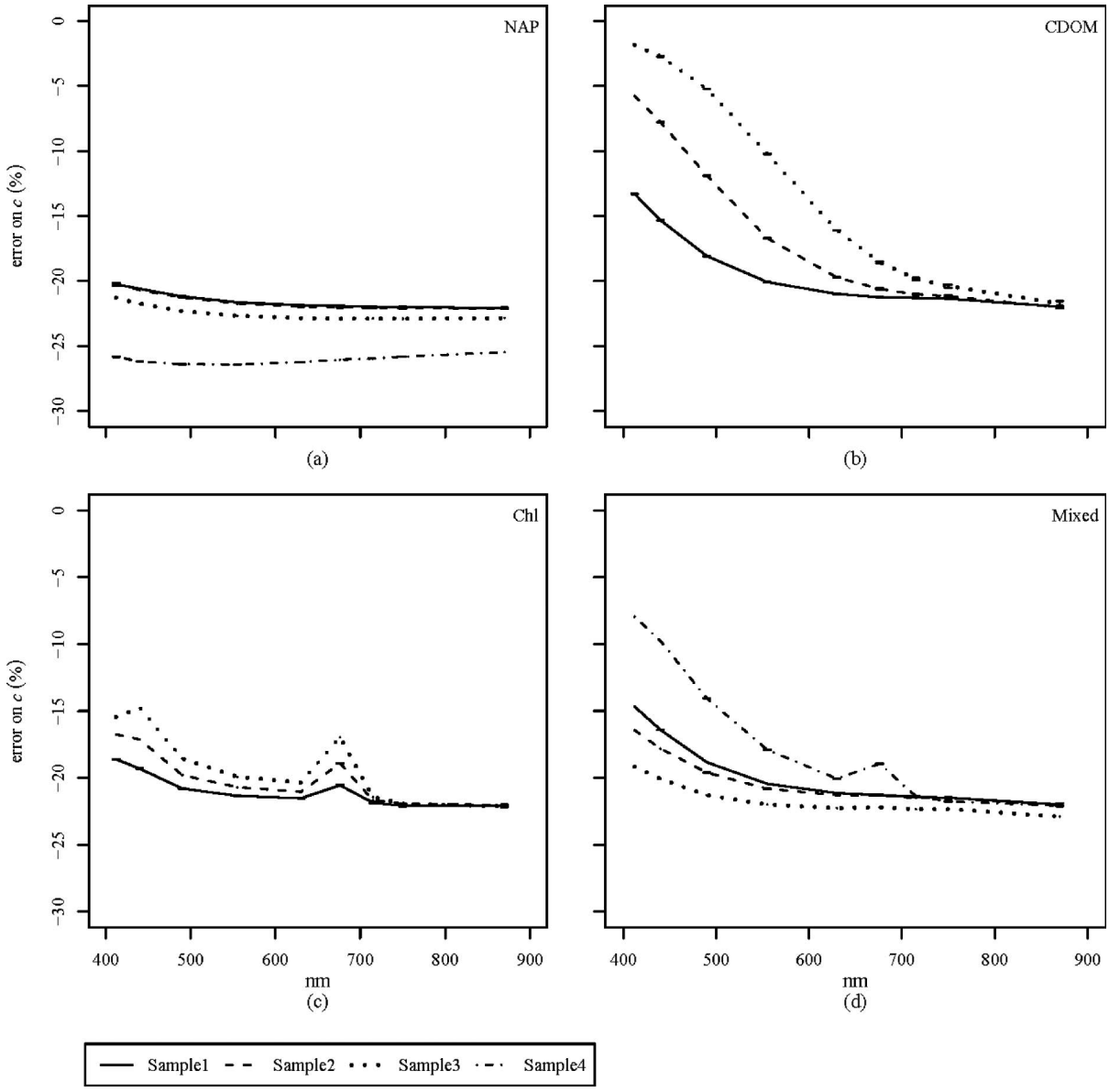

Fig. 4. Spectral errors associated with attenuation coefficients (c, in m^{-1}) measured in (a) NAP-dominated, (b) CDOM-dominated, (c) Chl-dominated, and (d) Mixed natural waters. For each water type, results are presented for sample1 to sample4. The AC-9 tube length is 10 cm, and the VSF used is FF-183.

absorption (i.e., ϖ_0 close to 1). Note that this result is strictly specific to the selected VSF (here FF-183). The underestimation of c_t is significantly reduced when light absorption becomes predominant over light scattering (i.e., ϖ_0 lower than 0.5). This typically occurs at short visible wavelengths, where CDOM strongly absorbs light [Figs. 4(b) and 4(d)], and around phytoplankton absorption peaks [Fig. 4(c)]. As the error mainly results from the collected scattered photons, the measured attenuation coefficients are quite accurate in the case of CDOM-dominated waters, which are essentially absorbing. In highly scattering waters ($b_t > 50$ m^{-1}, sample NAP4), the error on c_t slightly increases (26% underestimation, rather than 22%). This slight increase in the underestimation of c_t is due to multiple scattering effects [7]. Note again that these errors, which remain acceptable, are specific to the selected VSF. Large variations of k_c from 10% to 45% are expected based on the VSFs that have been documented in the literature [13,36,37].

We finally investigate how accurately the spectral slope of the attenuation coefficient can be retrieved from AC-9 measurements. This spectral slope is an important parameter, which, based on theory, is directly related to the particle size distribution in the case of nonabsorbing and homogeneous spherical particles following a power-law size distribution, with diameters ranging from 0 to infinity [38]. Particles found in mineral-rich coastal waters optically behave like such particles [39]. In our modeled NAP-dominated water samples, the spectral variations of c_t are well described ($R^2 > 0.99$) by a power-law function similar to the one presented in Eq. (14). Based on SimulO results, AC-9 measurements overestimate

the spectral slope of this power-law function by 5% on average and by up to 12% (Fig. 12). Those results validate the use of AC-9 measurements to study the particle size distribution in NAP-dominated waters.

B. Error on the Measured Absorption Coefficient

Several sources of error on a_t result from the adopted optical setup and are accounted for by the coefficient k_a. Additional sources of error result from the scattering correction method adopted here, i.e., from the assumptions made by Zaneveld *et al.* [2]. The first assumption is that k_a is flat spectrally. As a first approximation, k_a is obtained by integrating the normalized VSF beyond the critical angle of 41.7°. For the selected VSF (FF-183), this integral is equal to 7%. Our computations show that k_a values typically range from 9% to 13% (Fig. 5), i.e., values significantly higher than 7%. This is mainly due to the quartz tube length being shorter than the full path length (see Fig. 1). Even with a VSF spectrally flat over the considered wavelengths, k_a presents weak but significant spectral variations (maximum of 10% between 412 and 870 nm). These variations, multiplied by b_b, may significantly impact on the corrected absorption coefficient.

The variations of k_a are mainly related to the VSF, but are also induced by (not exhaustive):

i. the path length increase due to single and multiple scattering. It induces an overestimation of a_t, which depends on the level of scattering and is also almost proportional to the total absorption coefficient (i.e., including water). This effect is strong, especially at wavelengths associated with high light

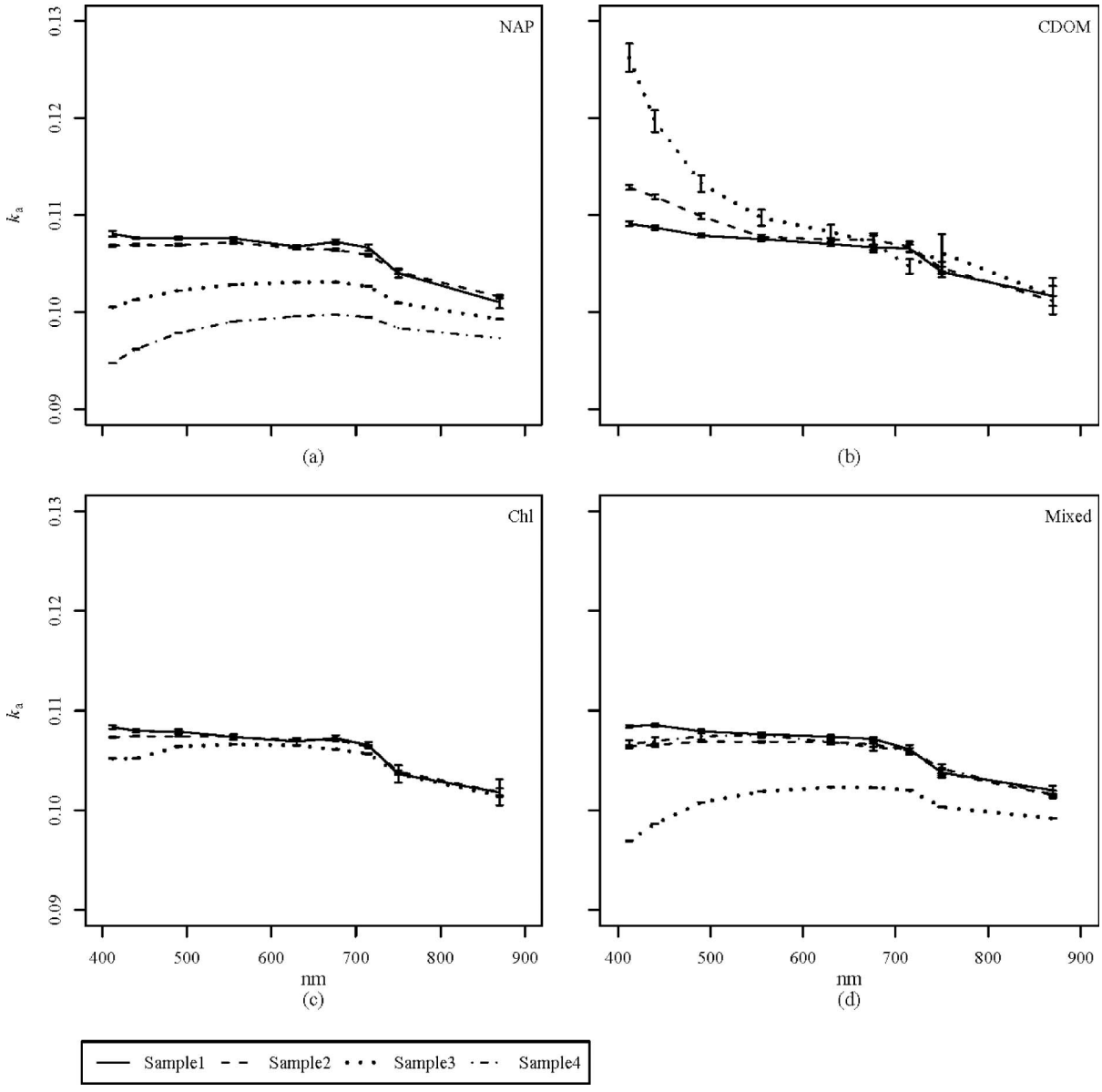

Fig. 5. Spectral variations of k_a in (a) NAP-dominated, (b) CDOM-dominated, (c) Chl-dominated, and (d) Mixed natural waters. For each water type, results are presented for sample1 to sample4. The AC-9 tube length is 10 cm, and the VSF used is FF-183.

absorption by pure water, and induces an increase of k_a with increasing a values;

ii. multiple reflections of photons at the extremities of the a-tube. This effect, already observed [40], is usually very weak, but becomes significant when scattering is low compared to absorption. It induces an increase of k_a with increasing light absorption [e.g., in the case of CDOM-dominated waters, Fig. 5(b)]. Note that the magnitude of this effect is highly sensitive to the modeling of the ends of the tubes (albedo of the extremities);

iii. multiple scattering, which enhances the divergence of the scattered beam so that less photons are collected at the end of the tube; or

iv. photons reflected by the quartz wall (quartz–air interface) of the a-tube, which could exhibit a shorter path length within the water sample due to the travel within the quartz wall (because the length traveled through the quartz wall shortens the travel within the water sample). Therefore, these photons are subject to limited absorption effects compared to photons traveling only within the water sample. This systematically results in the increase of k_a with decreasing light absorption and/or scattering.

It is difficult to assess theoretically the residual effect on k_a induced by these different processes. However, results of simulations show that photons traveling within the quartz wall of the tube are actually the predominant process controlling the variations of k_a for a wide range of IOPs. This is confirmed when simulating a quartz tube with a very thin wall. In such a case, the critical angle for total internal reflection at the quartz–air interface remains unchanged while the path length within the wall is negligible. For the same range of IOPs, results show that k_a increases as a or b increases when the quartz wall is thin (results not shown), while k_a decreases as a or b increases with the actual setup [Figs. 5(a), 5(c), and 5(d)]. Thus, removing this last effect while others remain unchanged is sufficient to modify the behavior of k_a.

In natural waters, the total scattering coefficient generally exhibits weak spectral variations, by opposition to the total absorption coefficient, which varies by several orders of magnitudes from short visible to near-IR wavelengths. It is, therefore, not so surprising that the spectral variations of k_a are related to the absorption spectrum. At 870 nm (highest pure water absorption coefficient at the considered wavelengths), k_a values are always lower than at 412 nm. An exception occurs when particulate light absorption at 412 nm is equivalent to light absorption by pure water at 870 nm (which only occurs for the NAP4 and Mixed3 samples). For the same reason, k_a is systematically higher at 715 nm than at 870 nm.

Therefore, the choice of the reference wavelength in the near-IR (where light absorption by pure water is high and strongly varies with wavelength) directly impacts on the spectral variation of k_a and, therefore, on the results obtained when applying the correction method for residual scattering [2]. Note that the CDOM-dominated waters represent a specific case [Fig. 5(b)]: k_a increases toward the short visible wavelength, as does light absorption. In such cases, associated with the lowest ϖ_0 values, the variations of k_a are mainly induced by the multiple reflections of photons at the extremities of the a-tube.

The errors on a_t depend on k_a variations, but also on the assumption of null absorption at the reference near-IR wavelength [2]. In our modeled samples, light absorption by the water constituents is zero at 870 nm, but not at 715 nm. The choice of the near-IR reference wavelength, therefore, impacts on the errors associated with a_t. Results from our simulations are presented when considering 870 then 715 nm as the reference near-IR wavelength (Fig. 6). The errors on a_t are only presented in the visible part of the spectrum, as the results obtained in the near-IR mainly depend on the assumption made at the reference wavelength.

When using 870 nm as the reference, errors are typically lower than 10% at short visible wavelengths (<450 nm). They increase toward red wavelengths and are at a maximum when absorption is close to zero, as the errors calculated are relative. The imperfect correction for residual scattering, due to the unexpected spectral variation of k_a, leads to errors of about 30% at 600 nm. As expected, the maximum errors correspond to the cases of highly scattering NAP-dominated waters [Fig. 6(a)]. In the case of CDOM-dominated waters (low scattering), the measured absorption values are much more accurate: errors are lower than 15% [Fig. 6(b)]. The case of Chl-dominated waters is of great interest as a representative of most oceanic waters. Around the phytoplankton absorption peaks (443 and 675 nm), errors are systematically lower than 10%. These errors increase between these wavelengths as the absorption coefficient is lower, but remain in the range of 10%–25%. The case of Mixed waters is also of high interest, as representative of most coastal waters. Once again, the errors remain limited (<15%) when 870 nm is used as the reference wavelength. In NAP-dominated waters, it is important to note that the computed relative errors on a_t depend on the spectral slope considered for a_{NAP} in Eq. (13). If, for example, a slope of 0.009 nm^{-1} is considered (instead of 0.0123 nm^{-1}), this results in higher a_{NAP} values at red and near-IR wavelengths, and, thus, in lower relative errors on a_t (e.g., 41% rather than 97% for sample NAP3 at 676 nm). But in terms of absolute errors on a_t (not shown), the differences are not really significant. The systematic overestimation of a_t is due to the fact that k_a or k_c are always lower at the near-IR reference wavelength than at any other wavelength. It is possible to show that a_t is overestimated when the F function defined by McKee *et al.* [41] (see their Eq. 4b), is over 1. This F function is equal to 1 at the reference near-IR wavelength and increases as k_a or k_c increases. The samples NAP4 and Mixed3 are two

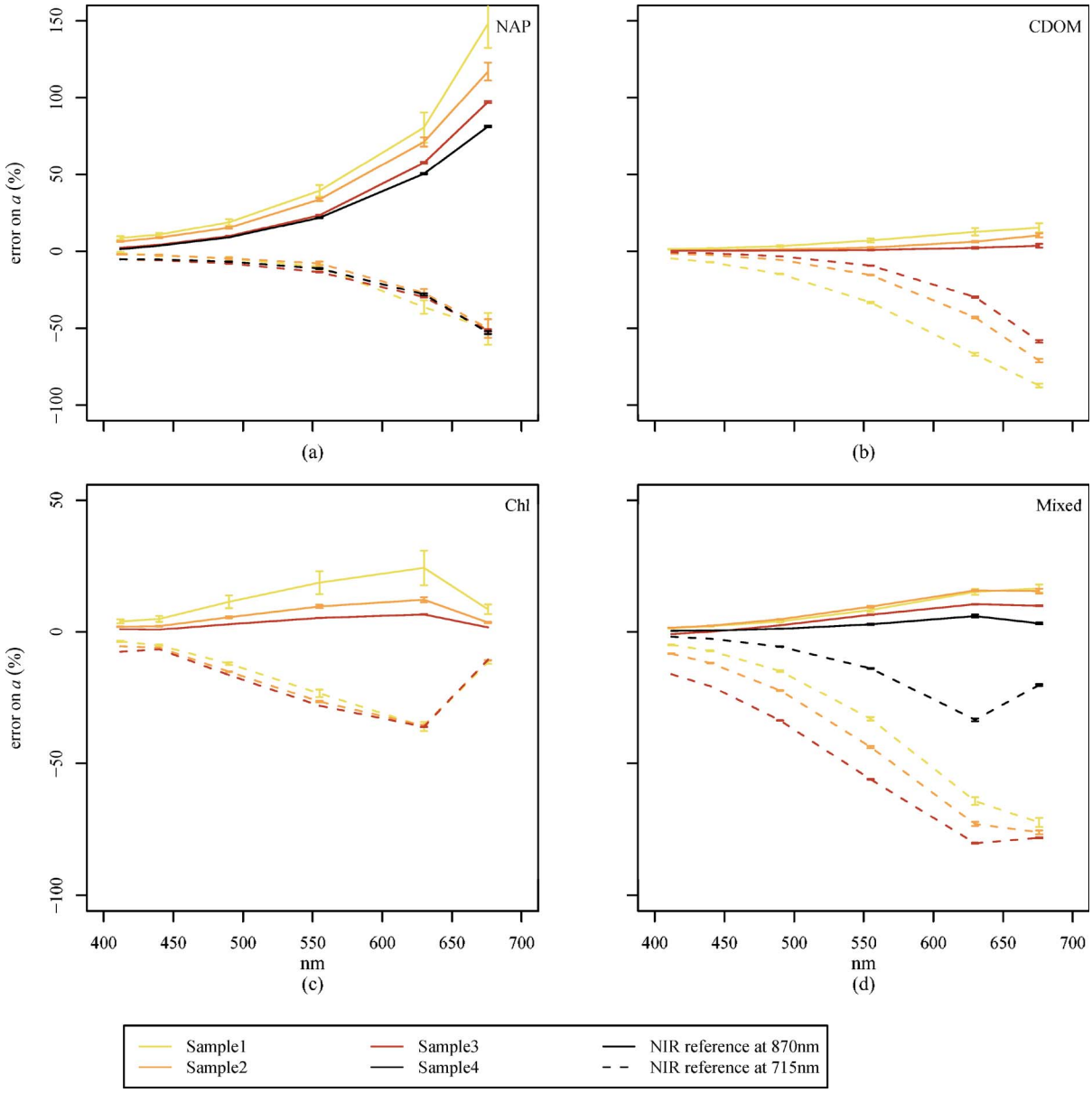

Fig. 6. (Color online) Spectral errors associated with absorption coefficients (a, in m^{-1}) measured in (a) NAP-dominated, (b) CDOM-dominated, (c) Chl-dominated, and (d) Mixed natural waters. For each water type, results are presented for sample1 to sample4. Results are presented when using 715 nm (dashed curves) or 870 nm (solid curves) as the reference near-IR wavelength. The AC-9 tube length is 10 cm, and the VSF used is FF-183.

atypical cases that both exhibit k_a values lower at 412 nm than at 870 nm. For these samples, the increase of k_c compensates for these low k_a values.

When using 715 nm (instead of 870 nm) as the reference near-IR wavelength, the errors are, as expected, higher in the red part of the spectrum and decrease toward shorter visible wavelengths. For Chl-dominated waters, errors are particularly low around phytoplankton peaks and are mostly independent, as for NAP-dominated waters, of the Chl (and/or NAP) concentration. The systematic underestimation of a_t is due to the residual absorption at 715 nm. When applying the so-called proportional method at a wavelength where absorption is not zero, Eq. (7) can be rewritten as

$$a_t(\lambda) = a_m(\lambda) - [a_m(\lambda_r) - a_t(\lambda_r)]\frac{b_m(\lambda)}{b_m(\lambda_r)} = a_c(\lambda) + a_t(\lambda_r)\frac{b_m(\lambda)}{b_m(\lambda_r)}, \quad (15)$$

where a_c is the absorption coefficient derived from Eq. (7). Equation (15) shows that the proportional method leads to an underestimation of a_t that is proportional to the absorption coefficient at the reference wavelength. For example, if we consider samples NAP3 and Mixed3, and if the assumption made in Eq. (6) is fulfilled, Eq. (15) leads to an underestimation of a_t at 412 nm by 3% and 14%, respectively. These values are only slightly lower than the

ones simulated. Therefore, Eq. (15) explains by itself the underestimation of a_t at short wavelengths due to residual absorption at λ_r.

We now look at the potential influence of the AC-9 tube length (10 or 25 cm) on the errors associated with absorption measurements. Simulations were carried out for the first two (less turbid) samples of each water type, for a 25 cm, then a 10 cm tube. Results show that the errors obtained remain comparable whatever the tube length [Figs. 7(c), 7(e), and 7(g)] except in the case of NAP-dominated waters [Fig. 7(a)]. In all cases, absorptions retrieved with a tube of 25 cm are slightly higher than those obtained with a tube of 10 cm. This is due to enhanced variations of k_a in the longer tube (Fig. 7, right panel). These variations of k_a induce an overestimation of a_t, which compensates for the underestimation resulting from the residual absorption at 715 nm. For NAP-dominated samples, this compensation is almost perfect. As the 25 cm length tube exhibits strong variations of k_a (induced by the spectral variations of the total absorption coefficient), such a tube length is not compatible with near-IR wavelengths around 870 nm (where light absorption by pure water varies by several orders of magnitude). The strong k_a variations from 870 nm to visible wavelengths would invalidate one of the main assumptions made in the proportional correction method (i.e., k_a could not be assumed to be flat spectrally).

Finally, we determined how accurately the spectral slope of the absorption coefficient can be retrieved from AC-9 measurements. To address this question, we considered the cases of NAP-dominated, CDOM-dominated, and Mixed waters, for which the spectral variation of the absorption coefficient is well described ($R^2 > 0.94$) by an exponential function [see Eqs. (12) and (13)]. The spectral slopes of the CDOM and NAP absorption coefficients are key parameters in marine optics, as they can be used as rough proxies for the chemical composition of the absorbing constituents. In NAP-dominated waters, the exponential spectral slope is rather poorly retrieved (typical error of −20%) due to imperfect corrections for residual scattering (Fig. 12). By opposition, in CDOM-dominated and Mixed waters, this spectral slope is retrieved with an error lower than 5% (slight underestimation). This is due to the low error on a_t [Figs. 6(b) and 6(d)].

C. Error on the Measured Scattering Coefficient

The estimation of errors on b_t is less explicit, as it results from the combined errors on c_t and a_t measurements [Eq. (2)]. Again, we discriminate the results obtained when using 715 or 870 nm as the reference near-IR wavelength in Eq. (7) (Fig. 8). The first observation is that errors are almost spectrally flat, in all cases. In NAP-dominated waters, the attenuation and scattering coefficients are very close, so that the errors on b_t and c_t are very similar: the b_c value underestimates by 22% the actual b_t value (up to 28% for the most turbid case). The same comment applies to Chl-dominated and Mixed waters, where b_t is typically 19% to 23% underestimated over the full spectrum considered (depending on the reference wavelength used). These results still hold in CDOM-dominated waters, when 870 nm is used as the reference wavelength in the near-IR. If 715 nm is used as the reference wavelength, the errors on b_t are significantly lower. This is due to the underestimation of a_t, which compensates for the underestimation of c_t. This compensation is particularly important for CDOM-dominated waters, as the magnitudes of b_t and a_t are similar. The error made on the scattering coefficient appears to be the most stable spectrally, thus *a priori* the easiest to predict if the VSF is known.

The spectral slope of the particulate scattering coefficient is another key parameter in marine optics, as it may be directly related to the size distribution of the hydrosols in the case of nonabsorbing particles distributed in size according to a power-law function [38]. Note that this assumption is usually not valid in the visible part of the spectrum [28,30]. Our computation results show that the value of the measured b_c spectral slope is systematically slightly underestimated, but only by a few percent (<5%) (Fig. 12). These results are valid whatever the water type considered (i.e., NAP, CDOM, Chl-dominated, and Mixed). The uncertainty on the measured spectral slope increases, but only up to −10%, in the case of the most scattering NAP-dominated waters and for the most absorbent CDOM sample.

D. Potential Impacts of Significant Particulate Absorption in the Near-IR and Variations of the VSF

In the previous computations, light absorption by particles was assumed to be negligible in the near-IR, i.e., $a_{\mathrm{NAP}}(870)$ and $a_{\mathrm{Chl}}(870)$ were both set to 0. This assumption, also made by Zaneveld *et al.* [2], relies on several studies dealing with natural particles [42,43], but remains questionable based on recent results [44,45]. The potential impact of significant light absorption by particles in the near-IR cannot be ignored in our study; it is investigated by considering a constant background B in Eq. (13), which becomes

$$a_{\mathrm{NAP}}(\lambda) = [\mathrm{NAP}] \times a^*_{\mathrm{NAP}}(440) \times (\exp(-0.0123 \times (\lambda - 440)) + B). \quad (16)$$

The B value was set to obtain a $a_{\mathrm{NAP}}(750) : a_{\mathrm{NAP}}(440)$ ratio of 25% and light absorption at 870 nm was no longer equal to zero. A ratio of 25% was considered in our computations based on measurements carried out in the North Sea, where the $a_{\mathrm{NAP}}(750) : a_{\mathrm{NAP}}(440)$ ratio was observed to vary between 18% and 24% [46]. The impact on the errors associated with the estimated k_a and k_c factors and the measured c_m and a_c coefficients are investigated using SimulO. Only the case of NAP-dominated waters is considered. Except for a_{NAP} [Eq. (16)], the IOPs parameterization for NAP samples (renamed samples NAPbkg1 to NAPbkg4) remains unchanged.

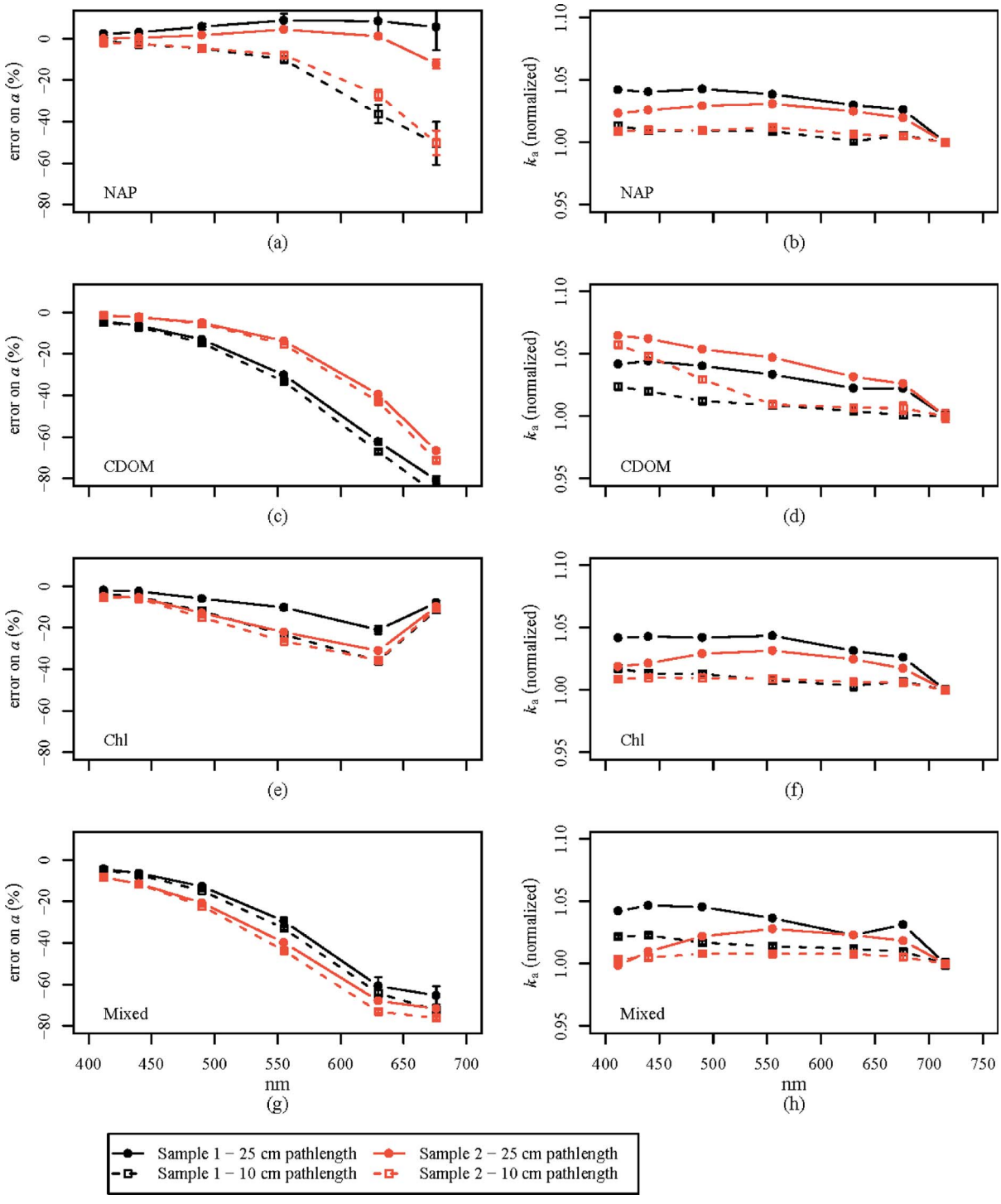

Fig. 7. (Color online) Spectral errors associated with absorption coefficients (a, in m^{-1}) depending on the length of the AC-9 tubes (10 or 25 cm). The errors are compared for the first two modeled samples of (a) NAP-dominated, (c) CDOM-dominated, (e) Chl-dominated, and (g) Mixed natural waters when using 715 nm as the reference near-IR wavelength. The corresponding spectral variations of k_a normalized at 715 nm are presented for each considered water type [(b), (d), (f), and (h), respectively]. The VSF used is FF-183.

The impact on the actual k_a values appears to be limited: k_a values still range between 9% and 11% and present similar spectral variations [see Fig. 9(a) as compared to Fig. 4(a)]. But errors on a_t raise dramatically: these errors are logically of −100% at the selected near-IR wavelength [see Eq. (9)], then gradually decrease in absolute values toward short visible wavelengths, but remain very high: −20%, −60%, and −75%, respectively at 412, 555, and 630 nm [Fig. 9(b)]. If the assumption of null particulate light absorption is not fulfilled in the near-IR, the proportional correction method leads to a dramatic underestimation of the absorption coefficient over the whole visible spectrum due to the residual term in

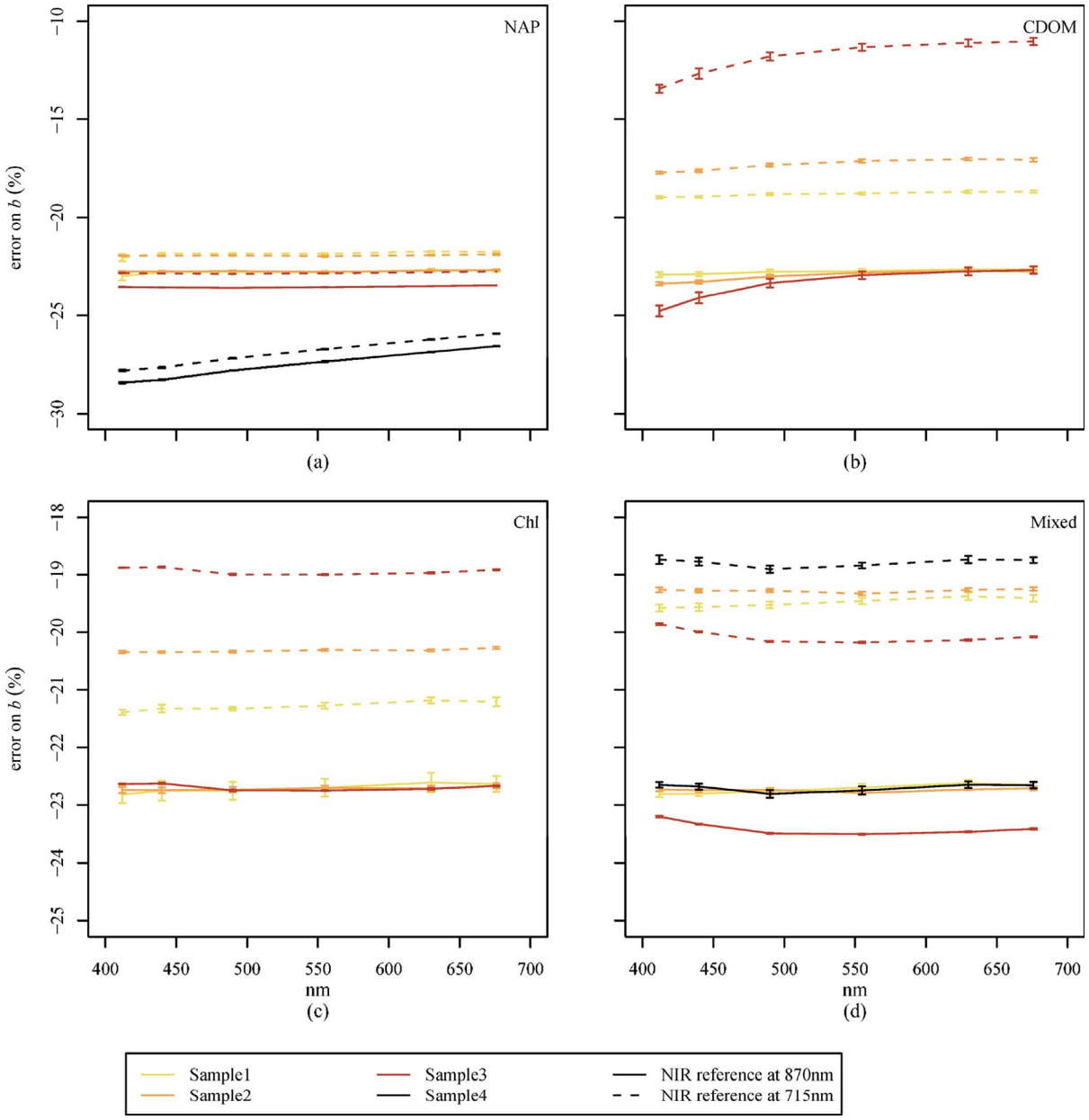

Fig. 8. (Color online) Spectral errors associated with scattering coefficients (b, in m^{-1}) in (a) NAP-dominated, (b) CDOM-dominated, (c) Chl-dominated, and (d) Mixed natural waters. For each water type, results are presented for sample1 to sample4. Results are presented when using 715 nm (dashed curves) then 870 nm (solid curves) as the reference near-IR wavelength. The AC-9 tube length is 10 cm, and the VSF used is FF-183.

Eq. (15). This would also have a dramatic impact on the retrieved a_t spectral slopes: the associated error, already important, would increase by a factor 5 (not shown). The results of our computations highlight the crucial need of accurate measurements of light absorption by particles in the near-IR spectral domain. The impact on k_c and c_m is much more limited and almost insignificant as the error on c_t mainly depends on the VSF. A possible significant light absorption by NAP would also have little impact on the accuracy of the c_t and b_t spectral slopes retrieved from AC-9 measurements (Fig. 12).

The impact on k_c and k_a, and on the resulting c_m and a_c coefficients induced by variations in the VSF of particles is finally investigated. This variation is described by a modification of the backscattering ratio used to create the Fournier–Forand phase function [34,35]. The cases of NAP- (NAP2 sample) and Chl- (Chl1 to Chl3 samples) dominated waters are considered. Values for the backscattering ratio are varied from 0.5% to 1.83% for Chl-dominated waters [36,47] and from 1% to 5% for NAP-dominated waters [48,49]. In NAP-dominated waters, variations of the particulate backscattering ratio (values of 5%, 1.83%, and 1%) lead to significant variations of k_c in terms of magnitude (9%, 22%, and 32%, respectively) while k_c remains flat spectrally [Fig. 10(c)]. This is because the changes in the angular distribution of

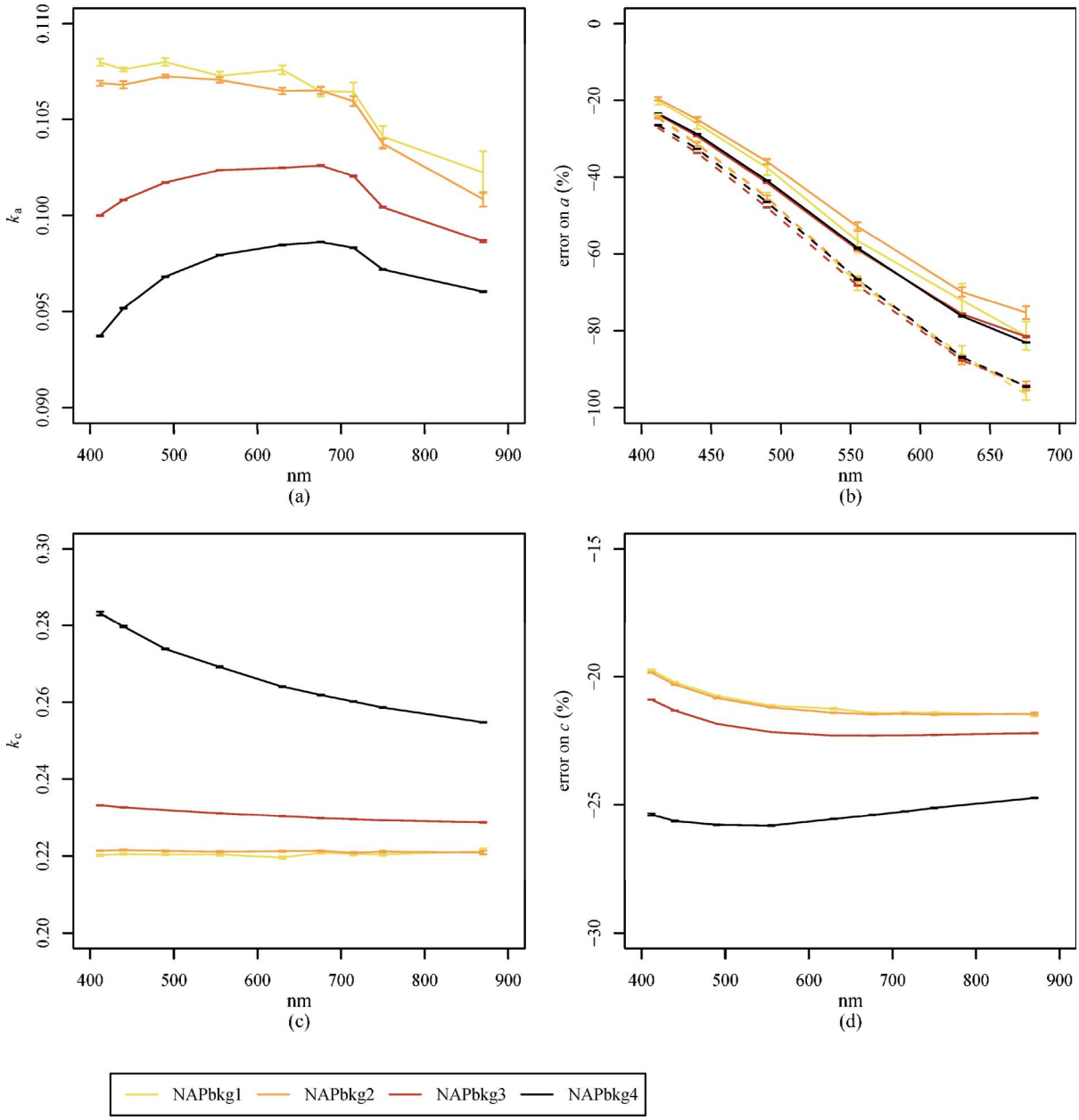

Fig. 9. (Color online) Spectral errors associated with (a) k_a, (b) a, (c) k_c, and (d) c when considering a background for the NAP absorption coefficient. The AC-9 tube length is 10 cm, and the VSF used is FF-183.

scattering only impact the fraction of scattered light detected by the detector of the c-tube. Consequently, the errors on c_t are −9%, −22%, and −32%, respectively [Fig. 10(d)]. It can be concluded, in agreement with McKee *et al.* [40], that the particulate backscattering ratio is the key parameter to be known *a priori* in order to accurately estimate k_c. Variations of this ratio also induce significant changes in the actual k_a values [Fig. 10(a)]: 7%, 11%, and 22%. These variations result in worse absorption retrieval [Fig. 10(b)] when light scattering is less peaked in the forward direction (higher backscattering ratio) and when using the scattering correction at 870 nm. By opposition, when using the scattering correction at 715 nm, the effect of the VSF is weaker.

The results are similar and consistent in the case of Chl-dominated waters. The variations of the particulate backscattering ratio (1.83%, 1%, and 0.5%) lead to significant variations of k_c in terms of magnitude (22%, 32%, and 44%, respectively) [Fig. 11(c)]. Again, these variations are simply because the fraction of scattered photons captured by the c detector increases when the VSF is highly peaked in the forward direction. The resulting errors on c_t are slightly lower than on k_c, i.e., they are respectively equal to −20%, −30%, and −42% [Fig. 11(d)]. k_c and the error on c_t do not strictly equal because of significant absorption on top of scattering; this significant light absorption induces weak spectral variations of the errors around the absorption peaks of

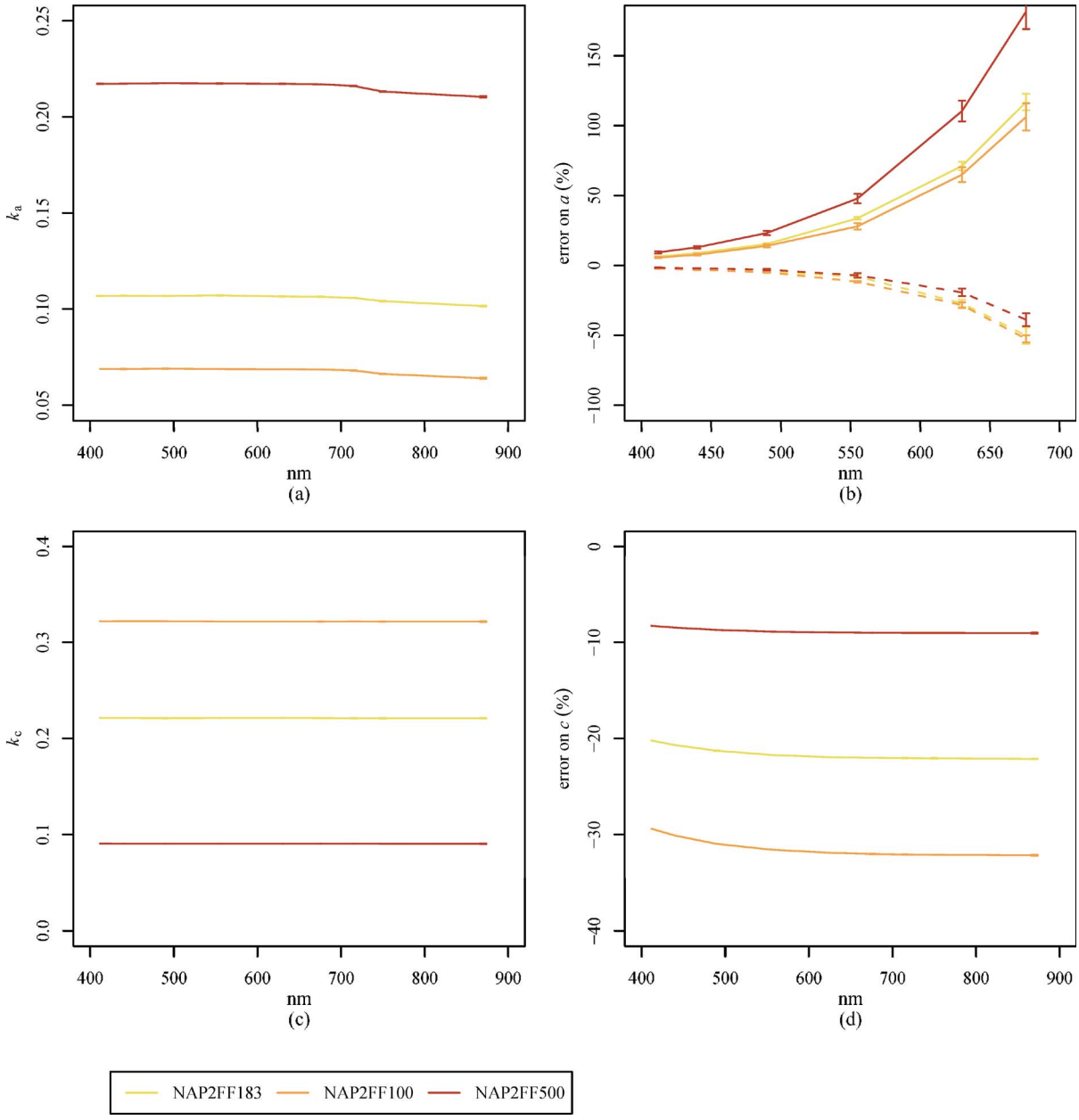

Fig. 10. (Color online) Spectral errors associated with (a) k_a, (b) a, (c) k_c, and (d) c when considering different scattering phase functions in the case of NAP-dominated natural waters. The AC-9 tubes length is 10 cm.

phytoplankton. In terms of k_a and errors on a_t, the results obtained in Chl- and NAP-dominated waters are simply concordant. When considering the scattering correction at 715 nm, the effect of the VSF is practically insignificant.

Based on our computations, the lack of knowledge on the actual VSF of Chl and NAP would have a significant impact on the accuracy of the retrieved spectral slopes of the a_t (for NAP samples), b_t, and c_t coefficients (Fig. 12).

E. General Guidance for Measurement Error Estimation

Our results provide estimations of the errors associated with the measured IOPs for a wide range of water types. These errors are complex. They result from the design of the AC-9 instrument and also from the scattering correction method. In our opinion, there is no general method that could allow a better IOPs retrieval without additional measurement, and the correction method proposed by Zaneveld *et al.* [2] is the most efficient. To estimate the errors associated with IOPs measured in the field, AC-9 users can use our results, which are representative for most natural waters. First, users must select the water type (NAP-, Chl-, or CDOM-dominated or Mixed) corresponding to their measurement based on ancillary data (e.g., Chl, suspended matter, and/or CDOM concentration) or prior knowledge of the IOPs of the sampled waters (open sea, coastal water). Then, within the selected water type, users can retrieve the modeled water sample corresponding to their sample by using absorption and scattering coefficients measured in the blue

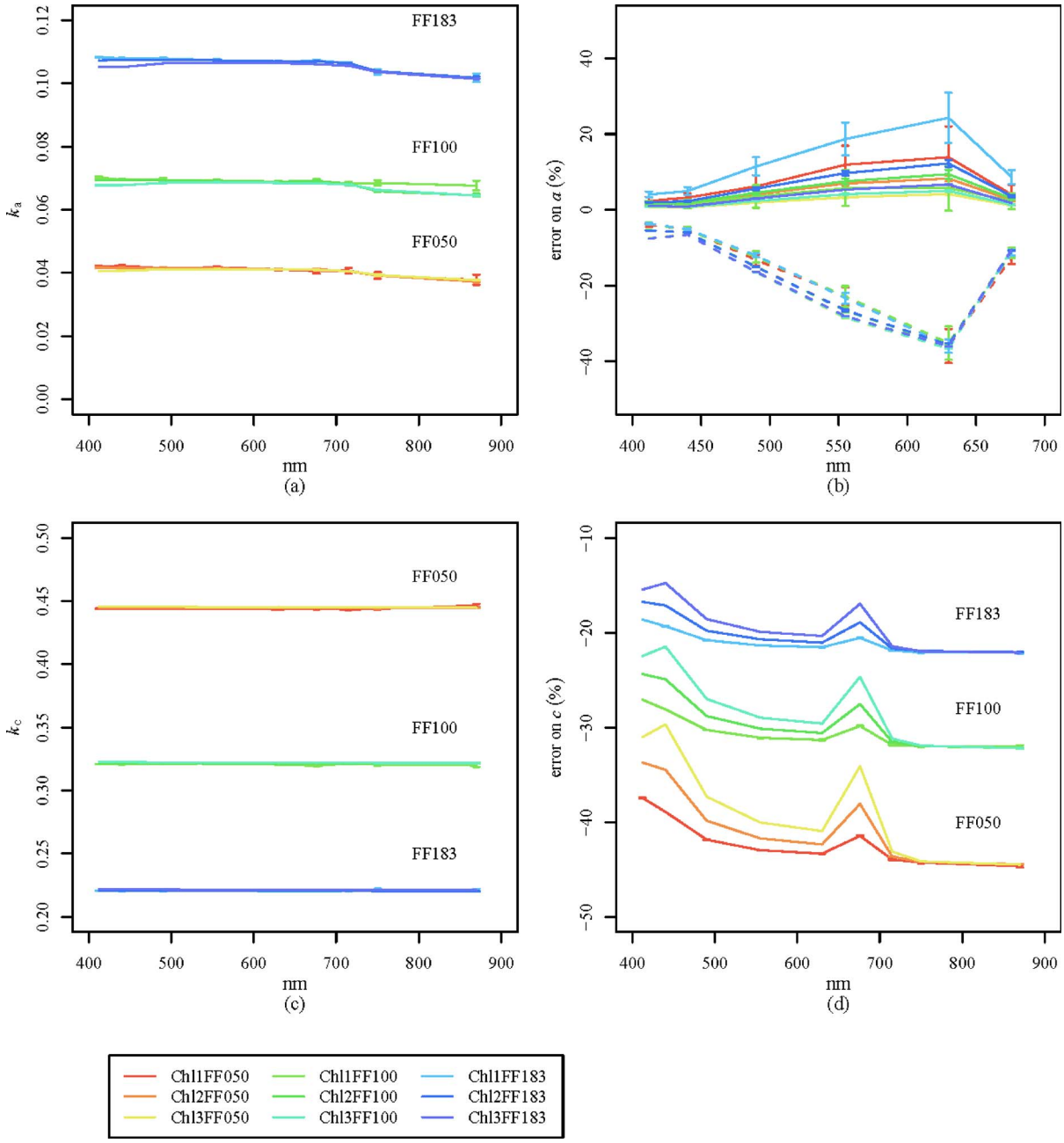

Fig. 11. (Color online) Spectral errors associated with (a) k_a, (b) a, (c) k_c, and (d) c when considering different scattering phase functions in the case of Chl-dominated natural waters. The AC-9 tubes length is 10 cm.

where the error on a and c is minimum. The comparison with the IOPs given in Fig. 2 will allow an interpolation of our errors on the different IOPs and their spectral variations. These errors will depend on the IOPs and VSF used as inputs in our simulations.

When measuring the attenuation coefficient, the key factor for error calculation is the shape of the VSF at small angles. This shape could be modeled for a given backscattering ratio [35] and integrated over the FOV of the detector to derive the k_c factor. In agreement with a recent study [7], we show that the simulated value is only slightly lower than the theoretical one, even in highly turbid waters. Then, according to the definition of this factor (Eq. 5), it is easy to derive the error on c_t.

When measuring the absorption coefficient, key factors are the near-IR wavelength used as reference in the scattering correction method (715 or 870 nm) and the value of the absorption coefficient at this wavelength. When using the scattering correction method at 870 nm, even with null absorption at this wavelength, we found a significant error due to the spectral variation of k_a. But, for all our samples that have a null absorption at 870 nm (i.e., excluding NAPbkg samples), there is a relationship between the error on a_t (for wavelengths lower than 715 nm)

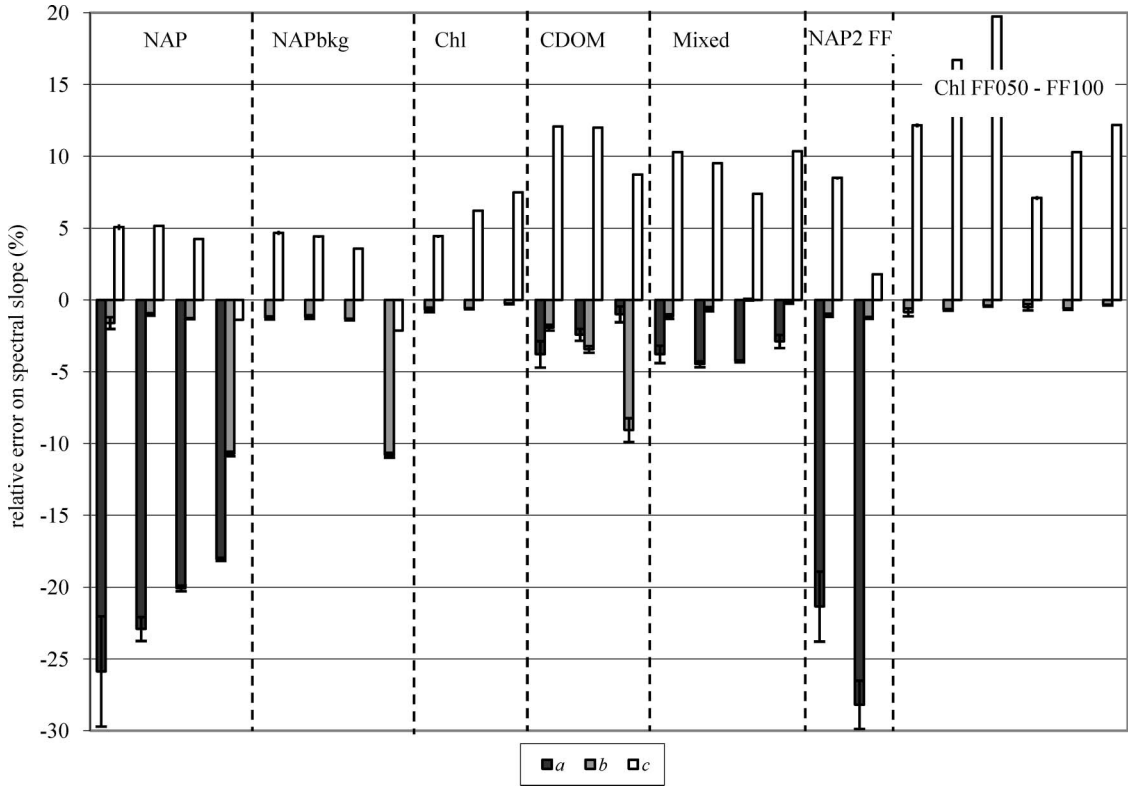

Fig. 12. Errors associated with the attenuation, absorption, and scattering spectral slopes modeled using a power-law function (for the scattering and attenuation coefficients) and an exponential function (for the absorption coefficient). Results are not presented for the water samples whose absorption spectra do not follow an exponential law as a function of wavelength (i.e., the cases of NAP background and Chl-dominated water samples are not considered here). Results from sample1 to sample4 are presented from the left to the right. The AC-9 tube length is 10 cm and 870 nm is used as the reference near-IR wavelength.

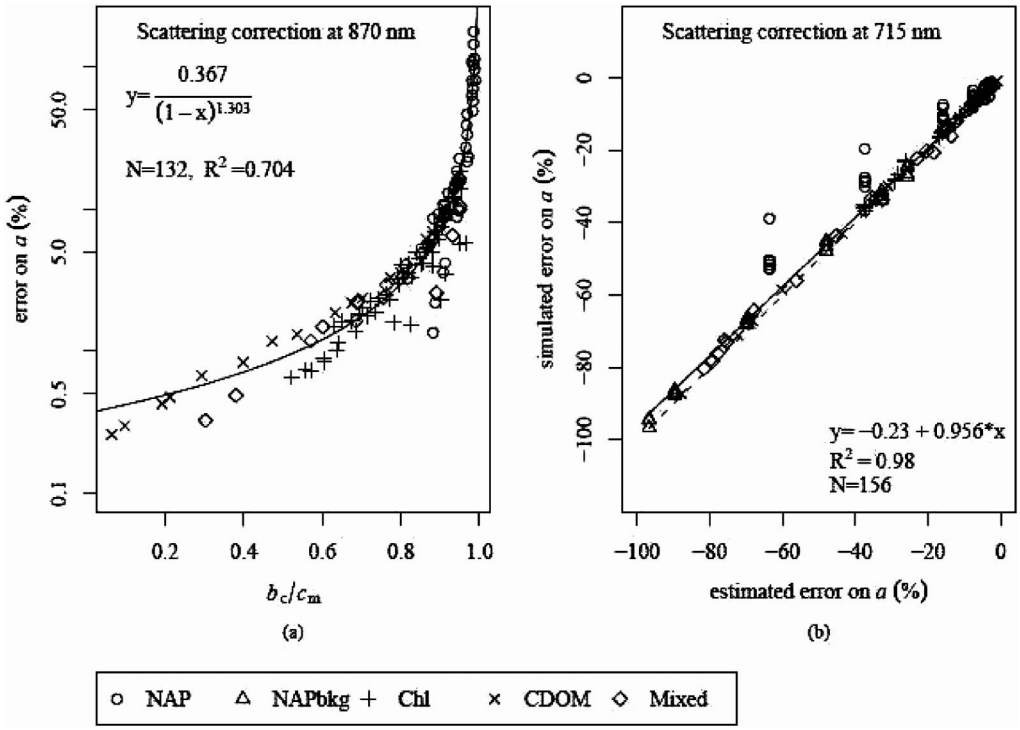

Fig. 13. (a) Error on a (%) as a function of b_c/c_m, when using 870 nm as the reference near-IR wavelength in the correction for residual scattering. (b) Error on a (%) as a function of the error on a estimated using Eq. (17), when using 715 nm as the reference near-IR wavelength in the correction for residual scattering. The AC-9 tube length is 10 cm [(a) and (b)]. Results are presented only at wavelengths below 700 nm for samples with a null absorption coefficient at 870 nm (a) and for all samples (b).

and the ratio b_c/c_m, which can be directly obtained from AC-9 measurements [Fig. 13(a)]. This relationship can be used to estimate the error for a given ratio b_c/c_m, then to correct the data for this error. By taking into account this relationship, the mean error on a_t decreases from 15% to 3%, while the global range of error moves from $[0, -180\%]$ to $[-20\%, -50\%]$. To apply this method, a user must be sure that there is no absorption at 870 nm, because, if it is not the case, it would correct for an assumed overestimation of a_t, while there is actually an underestimation of a_t. On the ontrary, when using the scattering correction method at 715 nm, it appears that the method of Zaneveld provides satisfactory results due to the limited variation of the absorption coefficient of pure water in the visible part of the spectrum. This results, for example, in a smaller variation of the error on a_t when changing the VSF than when using the scattering correction at 870 nm [Figs. 10(b) and 11(b)]. By using Eq. (15), it is possible to derive the theoretical error on a_t at a given wavelength due to the residual absorption:

$$\frac{a_c(\lambda) - a_t(\lambda)}{a_t(\lambda)} = -\frac{a_t(\lambda_r)}{a_t(\lambda)} \frac{b_t(\lambda)}{b_t(\lambda_r)}. \quad (17)$$

If we compare the simulated error and the one obtained by using this equation, for all our modeled samples including samples with absorption background in the near-IR (NAPbkg samples), we obtain a very good agreement [Fig. 13(b)]. Only NAP-dominated samples without absorption background in the near-IR present simulated errors lower than the estimated ones. This results from the strong error due to scattering effects in such samples as compared to residual absorption bias. Therefore, and by opposition to the scattering correction at 870 nm, the errors found mainly depend on the residual absorption at 715 nm, which is, in fact, related to our IOP assumptions. Obviously, it is not possible to correct data for this effect because $a_t(\lambda_r)$ is unknown *a priori*. But Eq. (17) can be used to estimate error on absorption for any user's IOP dataset.

5. Conclusion

Monte Carlo simulations were performed to explain and quantify the errors associated with the attenuation, absorption, and scattering coefficients that can be measured in natural waters using a WET Labs AC-9 and/or AC-S device. The errors quantified are the ones related to the design of the sensor and result from imperfect corrections for scattering effects. Both the visible and near-IR spectral domains were considered. Computations were performed for tube lengths of 10 and 25 cm.

Results confirm that the attenuation coefficient could be accurately measured if the particle VSF was known. As this is usually not the case, the measured attenuation coefficient is typically underestimated by 10% and up to 40%, depending on the actual VSF. In waters where particle scattering dominates the optical properties, these errors are rather flat spectrally. This is no longer true in waters associated with strong light absorption by the colored water constituents (e.g., CDOM-dominated waters).

Table 1. List of Symbols

Symbol	Parameter and Unit
λ	Light wavelength in vacuum (nm)
λ_r	Reference near-IR wavelength for scattering correction [2] (nm)
a	Total absorption coefficient (m^{-1})
a_w	Pure seawater absorption coefficient (m^{-1})
a_{NAP}	Absorption coefficient of non-algal particles (m^{-1})
a^*_{NAP}	Mass-specific absorption coefficient of non-algal particles (m^2 g^{-1})
a_{CDOM}	Absorption coefficient of colored dissolved organic matter (m^{-1})
a_{Chl}	Absorption coefficient of phytoplankton particles (m^{-1})
a^*_{Chl}	Chlorophyll-specific absorption coefficient of phytoplankton (m^2(mg Chl)$^{-1}$)
a_t	Absorption coefficient of colored water constituents on top of pure water assigned (true) to each modeled water sample (m^{-1})
a_m	Absorption coefficient measured by the simulated AC-9 (m^{-1})
a_c	Absorption coefficient retrieved after scattering correction [2] of the measured a_m coefficient(m^{-1})
b	Total scattering coefficient (m^{-1})
b_b	Particulate backscattering coefficient (m^{-1})
b_w	Pure seawater scattering coefficient (m^{-1})
b_{Chl}	Scattering coefficient of phytoplankton particles (m^{-1})
b_{NAP}	Scattering coefficient of non-algal particles (m^{-1})
b^*_{NAP}	Mass-specific scattering coefficient of non-algal particles (m^2 g^{-1})
b_t	Scattering coefficient of optically active water constituents on top of pure water assigned (true) to each modeled water sample (m^{-1})
b_m	Scattering coefficient measured by the simulated AC-9, obtained from the difference $c_m - a_m$ (m^{-1})
b_c	Scattering coefficient retrieved after scattering correction [2] expressed as $c_m - a_c$ (m^{-1})
c	Total attenuation coefficient expressed as $a + b$ (m^{-1})
c_t	Attenuation coefficient obtained as $a_t + b_t$ (m^{-1})
c_m	Attenuation coefficient measured with the simulated AC-9 (m^{-1})
x	Variation coefficient a, b, or c (m^{-1})
ϖ_0	Single scattering albedo (dimensionless)
$P^x_{a_t,b_t}$	Probabilities of detection (number of photons detected divided by the number of photons emitted) for the x-tube and for a given set of inherent optical properties (dimensionless)
L	AC-9 tube length (m)
FOV	Detector field of view (degree, half angle)
k_a	Scattering error coefficient in the absorption tube, expressed as $(a_m - a_t)/b_t$ (dimensionless)
k_c	Scattering error coefficient in the attenuation tube, expressed as $(c_t - c_m)/b_t$ (dimensionless)

Table 2. List of Modeled Water Samples

Name	Description
NAPn	Water samples whose inherent optical properties are dominated by those of non-algal particles ($n = 1, 2, 3,$ or 4)
NAPbkgn	Water samples whose inherent optical properties are dominated by those of non-algal particles with significant particulate light absorption in the near-IR spectral region ($n = 1, 2, 3,$ or 4)
Chln	Water samples whose inherent optical properties are dominated by those of phytoplankton particles ($n = 1, 2,$ or 3)
CDOMn	Water samples whose inherent optical properties are dominated by those of colored dissolved organic matter ($n = 1, 2,$ or 3)
Mixedn	Water samples whose inherent optical properties result from the mixed contributions of the different colored water constituents ($n = 1, 2, 3,$ or 4)
FF-xxx	Fournier–Forand phase function with a backscattering ratio of x.xx%
NAP2FFxxx	NAP2 sample with a FF-xxx Fournier–Forand phase function
ChlnFFxxx	Chln sample with a FF-xxx Fournier–Forand phase function

The main problem associated with AC-9 and AC-S measurements concerns the correction for residual scattering in the reflecting tube used to measure light absorption. The actual k_a and k_c coefficients, assumed to be wavelength independent in the proportional correction method [2], do vary spectrally, mostly due to spectral variations of the total absorption coefficient (including absorption by pure water) and because of photons traveling within the quartz wall of the a-tube. As a consequence, the relative errors on the resulting absorption coefficients vary from 5% to 10% where light absorption by the optically active water constituents is high enough (e.g., at short visible wavelengths and around phytoplankton absorption peaks) and increase in the red and near-IR regions, especially in NAP-dominated waters. These errors become dramatic if the assumption of negligible non-water absorption in the near-IR is not fulfilled. An accurate knowledge of particulate absorption in this spectral region is definitely a crucial point, especially for coastal waters [43–45]. Despite this significant uncertainty on absorption measurements, accurate estimations of the particulate scattering coefficient (if the actual VSF is known) and scattering spectral slope are possible. Moreover, it is interesting to note that the extremely high scattering that occurs in turbid coastal waters does not represent a strong limit for field spectrophotometric measurements of light attenuation and scattering.

This study has highlighted the potential but also the limits of current field spectrophotometers that have been used intensively during the past years to study the IOPs of natural waters. At this point, we simply conclude that the existing datasets should be reconsidered, taking into account the uncertainties documented in this paper. Further research is required to measure in the field (i) the actual VSF of marine particles and (ii) particulate light absorption in the near-IR spectral region.

This study was funded by a European Reintegration Grant (contract ERG-14905 RSFLUX), the Centre National d'Etudes Spatiales (CNES-France), and the BELCOLOUR-2 project (funded by the Belgian Science Policy Office STEREO-2 programme). We thank also two anonymous reviewers for their helpful comments.

References

1. D. Antoine, F. d'Ortenzio, S. B. Hooker, G. Bécu, B. Gentili, D. Tailliez, and A. J. Scott, "Assessment of uncertainty in the ocean reflectance determined by three satellite ocean color sensors (MERIS, SeaWiFS and MODIS-A) at an offshore site in the Mediterranean Sea (BOUSSOLE project)," J. Geophys. Res. **113**, C07013 (2008).
2. J. R. V. Zaneveld, J. C. Kitchen, and C. M. Moore, "The scattering error correction of reflecting-tube absorption meters," Proc. SPIE **2258**, 44–55 (1994).
3. J. R. V. Zaneveld, J. C. Kitchen, A. Bricaud, and C. C. Moore, "Analysis of in-situ spectral absorption meter data," Proc. SPIE **1750**, 187–200 (1992).
4. S. Pegau, D. Gray, and J. R. V. Zaneveld, "Absorption and attenuation of visible and near-infrared light in water: dependence on temperature and salinity," Appl. Opt. **36**, 6035–6046 (1997).
5. V. S. Langford, A. J. McKinley, and T. I. Quickenden, "Temperature dependence of the visible-near-infrared absorption spectrum of liquid water," J. Phys. Chem. A **105**, 8916–8921 (2001).
6. J. M. Sullivan, M. S. Twardowski, J. R. V. Zaneveld, C. M. Moore, A. H. Barnard, P. L. Donaghay, and B. Rhoades, "Hyperspectral temperature and salt dependence of absorption by water and heavy water in the 450–750 nm spectral range," Appl. Opt. **45**, 5294–5309 (2006).
7. J. Piskozub, D. Stramski, E. Terril, and W. K. Melville, "Influence of forward and multiple light scatter on the measurements of beam attenuation in highly scattering marine environments," Appl. Opt. **43**, 4723–4731 (2004).
8. J. R. V. Zaneveld and R. Bartz, "Beam attenuation and absorption meters," Proc. SPIE **489**, 318–324 (1984).
9. K. J. Voss and R. W. Austin, "Beam attenuation measurement error due to small-angle scattering acceptance," J. Atmos. Ocean. Technol. **10**, 113–121 (1993).
10. E. Boss, W. H. Slade, M. Behrenfeld, and G. Dall'Olmo, "Acceptance angle effects on the beam attenuation in the ocean," Opt. Express **17**, 1535–1550 (2009).
11. J. T. O. Kirk, "Point-source integrating-cavity absorption meter: theoretical principles and numerical modelling," Appl. Opt. **36**, 6123–6128 (1997).
12. R. A. Leathers, T. V. Downes, and C. O. Davis, "Analysis of a point-source integrating-cavity absorption meter," Appl. Opt. **39**, 6118–6127 (2000).
13. T. J. Petzold, "Volume scattering functions for selected ocean waters," Contract No. N62269-71-C-0676, UCSD, SIO Ref. 72–78 (Scripps Institution of Oceanography, 1972).
14. J. T. O. Kirk, "Monte Carlo modeling of the performance of a reflective tube absorption meter," Appl. Opt. **31**, 6463–6468 (1992).

15. C. D. Mobley, B. Gentili, H. R. Gordon, Z. Jin, G. W. Kattawar, A. Morel, P. Reinersman, K. Stamnes, and R. H. Stavn, "Comparison of numerical models for computing underwater light fields," Appl. Opt. **32**, 7484–7504 (1993).
16. J. Piskozub, P. J. Flatau, and J. R. V. Zaneveld, "Monte Carlo study of the scattering error of a quartz reflective absorption tube," J. Atmos. Ocean. Technol. **18**, 438–445 (2001).
17. R. M. Pope and E. S. Fry, "Absorption spectrum (380–700 nm) of pure water," Appl. Opt. **36**, 8710–8723 (1997).
18. L. H. Kou, D. Labrie, and P. Chylek, "Refractive indices of water and ice in the 0.65 to 2.5 μm spectral range," Appl. Opt. **32**, 3531–3540 (1993).
19. A. Morel, "Optical properties of pure water and pure seawater," in *Optical Aspects of Oceanography*, N. G. Jerlov and E. S. Nielsen, eds. (Academic, 1974), pp. 1–24.
20. X. Zhang, L. Hu, and M. X. He, "Scattering by pure seawater: effect of salinity," Opt. Express **17**, 5698–5710 (2009).
21. L. Prieur and S. Sathyendranath, "An optical classification of coastal and oceanic waters based on the specific spectral absorption curves of phytoplankton pigments, dissolved organic matter, and other particulate materials," Limnol. Oceanogr. **26**, 671–689 (1981).
22. A. Bricaud, M. Babin, A. Morel, and H. Claustre, "Variability in the chlorophyll-specific absorption coefficient of natural phytoplankton: analysis and parametrization," J. Geophys. Res. **100**, 13321–13332 (1995).
23. G. Dall'Olmo and A. A. Gitelson, "Effect of bio-optical parameter variability on the remote estimation of chlorophyll-a concentration in turbid productive waters: experimental results," Appl. Opt. **44**, 412–422 (2005).
24. H. R. Gordon and A. Morel, "Remote assessment of ocean color for interpretation of satellite visible imagery, a review," *Lecture Notes on Coastal and Estuarine Studies* (Springer Verlag, 1983), Vol. 4.
25. A. Bricaud, A. Morel, and L. Prieur, "Absorption by dissolved organic matter of the sea (yellow substance) in the UV and visible domains," Limnol. Oceanogr. **26**, 43–53 (1981).
26. M. Babin, D. Stramski, G. M. Ferrari, H. Claustre, A. Bricaud, G. Obolensky, and N. Hoepffner, "Variations in the light absorption coefficients of phytoplankton, non-algal particles, and dissolved organic matter in coastal waters around Europe," J. Geophys. Res. **108**, 3211–3230 (2003).
27. C. S. Roesler, M. J. Perry, and K. L. Carder, "Modeling in situ phytoplankton absorption from total absorption spectra in productive inland marine waters," Limnol. Oceanogr. **34**, 1510–1523 (1989).
28. M. Babin, A. Morel, V. Fournier-Sicre, F. Fell, and D. Stramski, "Light scattering properties of marine particles in coastal and oceanic waters as related to the particle mass concentration," Limnol. Oceanogr. **48**, 843–859 (2003).
29. S. Sathyendranath, L. Prieur, and A. Morel, "A 3 component model of ocean color and its application to remote-sensing of phytoplankton pigments in coastal waters," Int. J. Remote Sens. **10**, 1373–1394 (1989).
30. D. Doxaran, K. Ruddick, D. McKee, B. Gentili, D. Tailliez, M. Chami, and M. Babin, "Spectral variations of light scattering by marine particles in coastal waters, from the visible to the near infrared," Limnol. Oceanogr. **54**, 1257–1271 (2009).
31. A. Morel and L. Prieur, "Analysis of variations in ocean color," Limnol. Oceanogr. **22**, 709–722 (1977).
32. D. Doxaran, R. C. N. Cherukuru, and S. J. Lavender, "Apparent and inherent optical properties of turbid estuarine waters: measurements, empirical quantification relationships, and modeling," Appl. Opt. **45**, 2310–2324 (2006).
33. A. Bricaud, A. Morel, M. Babin, K. Allali, and H. Claustre, "Variations of light absorption by suspended particles with the chlorophyll a concentration in oceanic (Case 1) waters: analysis and implications for bio-optical models," J. Geophys. Res. **103**, 31033–31044 (1998).
34. G. Fournier and J. L. Forand, "Analytic phase function for ocean water," Proc. SPIE **2258**, 194–201 (1994).
35. C. D. Mobley, L. K. Sundman, and E. Boss, "Phase function effects on oceanic light fields," Appl. Opt. **41**, 1035–1050 (2002).
36. M. S. Twardowski, E. Boss, J. B. Macdonald, W. S. Pegau, A. H. Barnard, and J. R. V. Zaneveld, "A model for estimating bulk refractive index from the optical backscattering ratio and the implications for understanding particle composition in case I and case II waters," J. Geophys. Res. **106**, 14129–14142 (2001).
37. J. M. Sullivan and M. S. Twardowski, "Angular shape of the oceanic particulate volume scattering function in the backward direction," Appl. Opt. **48**, 6811–6819 (2009).
38. A. Morel, "Light scattering by seawater. Experimental results and theoretical approach," in *Optics of the Sea*, AGARD Lecture Series (NATO, 1973), pp. 3.1.1–3.1.76.
39. E. Boss, M. S. Twardowski, and S. Herring, "Shape of the particulate beam attenuation spectrum and its inversion to obtain the shape of the particulate size distribution," Appl. Opt. **40**, 4885–4893 (2001).
40. D. McKee, J. Piskozub, and I. Brown, "Scattering error corrections for in situ absorption and attenuation measurements," Opt. Express **16**, 19480–19492 (2008).
41. D. McKee, A. Cunningham, and S. Craig, "Semi-empirical correction algorithm for AC-9 measurements in a coccolithophore bloom," Appl. Opt. **42**, 4369–4374 (2003).
42. M. Babin and D. Stramski, "Light absorption by aquatic particles in the near-infrared spectral region," Limnol. Oceanogr. **47**, 911–915 (2002).
43. M. Babin and D. Stramski, "Variations in the mass-specific absorption coefficient of mineral particles suspended in water," Limnol. Oceanogr. **49**, 756–767 (2004).
44. S. Tassan and G. M. Ferrari, "Variability of light absorption by aquatic particles in the near-infrared spectral region," Appl. Opt. **42**, 4802–4810 (2003).
45. R. Röttgers, A. Bracher, S. Gehnke, B. Schmitt, and S. Wozniak, "Light absorption by natural aquatic particles in the near-infrared (700–900 nm) spectral region," presented at Ocean Optics XIX conference, Barga, Italy, 6 October 2008.
46. R. Röttgers, Institute for Coastal Research, GKSS Research Center Geesthacht, Max-Planck-Strasse 1, D-21502 (personal communication, 2010).
47. H. Loisel, X. Mériaux, J. F. Berthon, and A. Poteau, "Investigation of the optical backscattering to scattering ratio of marine particles in relation to their biogeochemical composition in the eastern English Channel and southern North Sea," Limnol. Oceanogr. **52**, 739–752 (2007).
48. D. McKee and A. Cunningham, "Identification and characterisation of two optical water types in the Irish Sea from in situ inherent optical properties and seawater constituents," Estuar. Coast. Shelf Sci. **68**, 305–316 (2006).
49. D. McKee, M. Chami, I. Brown, V. Sanjuan Calzado, D. Doxaran, and A. Cunningham, "Role of measurement uncertainties in observed variability in the spectral backscattering ratio: a case study in mineral-rich coastal waters," Appl. Opt. **48**, 4663–4675 (2009).